scientific reports

Check for updates

OPEN

Exploring the efficacy of *Benincasa hispida* extract on obesity linked inflammatory bowel disease by integrating computational analysis and experimental validations

Santosh B. Patil[1], Manisha B. Kuvalekar[1], Deepak A. Yaraguppi[2]✉, D. S. N. B. K. Prasanth[3], Sangameshwar G. Halkavatagi[1], Gururaj B. Tennalli[2], Mukhatar Ahmed Javali[4] & T. M. Yunus Khan[5,6]

The association of obesity with inflammatory bowel disease (IBD) can be understood by the intricate role of pro- and anti-inflammatory cytokines, especially adipokines, which are secreted by adipose tissue and are responsible for IBD because of their structural similarity with tumor necrosis factor-alpha (TNF-α), an important cytokine involved in IBD pathogenesis. The current study was carried out to evaluate the therapeutic potential of *Benincasa hispida* in obesity-associated IBD. Approximately 18 compounds sourced from *Benincasa hispida* (Thunb.) were comprehensively analyzed, among which 11 presented favorable drug-likeness scores and adherence to Lipinski's Rule of Five. Various methodologies, including compound-gene set pathway enrichment analysis, network pharmacology, docking studies, and molecular dynamics simulations, have been employed. Safety assessments via Protox confirmed the nontoxic nature of these compounds, which is crucial for their therapeutic potential. Through Venn diagram analysis of the Gene Card and OMIM databases, proteins associated with obesity and IBD management were pinpointed. Pathway enrichment analysis revealed 810 targets across 192 distinct pathways, with 8 directly related to the pathogenesis of obesity and IBD. Notable therapeutic targets, such as MTOR, were identified through STRING and KEGG pathway database analyses, shedding light on the molecular pathways modulated by these protein targets. Interactions among compounds, proteins, and pathways were visualized via Cytoscape 3.6.1. Furthermore, the compounds were docked with the protein target via AutoDock 4.2, and the compound ajmalin exhibited the highest binding affinity with the MTOR protein, with a binding energy of -7.8 kcal/mol; later, a dynamic study was performed for the ajmaline and protein complex. These findings shed light on the potential efficacy of *Benincasa hispida* in targeting crucial pathways for managing obesity and IBD. Hence, in vivo studies involving Wistar rats exposed to microplastics and monosodium glutamate (MSG) were carried out to evaluate the potential of *Benincasa hispida* extracts in mitigating obesity-related IBD. Fecal lipid analysis revealed alterations associated with these conditions, whereas histopathological examinations of the liver and intestine revealed the inflammatory changes induced by MSG and microplastics. The protective effects of this extract on liver and intestinal histology suggest promising avenues for further investigations, emphasizing its potential as a therapeutic intervention for IBD and obesity.

Keywords Obesity, IBD, *Benincasa hispida*, Network pharmacology, Molecular Docking, Molecular dynamics, Monosodium glutamate, Microplastic

[1]KLE College of Pharmacy, Hubballi 580031, Karnataka, India. [2]Department of Biotechnology, KLE Technological University, Hubballi 580031, Karnataka, India. [3]School of Pharmacy and Management, SVKM's Narsee Monjee Institute of Management Studies, Polepaly SEZ TSIIC, Jadcherla, Hyderabad 509301, Mahbubnagar, Telangana, India. [4]Department of periodontics and community dental science, Division of Periodontics, College of Dentistry, Abha Asir Region, King Khalid University, Abha, Saudi Arabia. [5]Central Labs, King Khalid University, P.O. Box 960,

AlQuara'a, Abha, Saudi Arabia. [6]Department of Mechanical Engineering, College of Engineering, King Khalid University, Abha 61421, Saudi Arabia. ✉email: deepak.yaraguppi@gmail.com

Inflammatory bowel disease (IBD), a chronic gastrointestinal disorder, is characterized by multiple intra- and extraintestinal manifestations, including autoimmune phenomena, intestinal inflammation, and mucosal tissue damage that are triggered and sustained by an imbalanced immune response. It encompasses two main types: ulcerative colitis (UC), characterized by persistent inflammation in a specific area of the digestive tract, and Crohn's disease (CD), which causes inflammation anywhere along the lining of the digestive tract, particularly in the colon. Abdominal pain, diarrhea, bloody stools, and vomiting are some of the symptoms of IBD. IBD is induced by environmental variables that affect genetically sensitive hosts. Although immunologic, environmental, and genetic factors may all play a role in the disease process, the exact causes of IBD, including CD and UC, are still unknown[1]. Obesity is a condition characterized by excessive fat accumulation in adipose tissue and ongoing, low-grade inflammation, which results from a complex interplay between genetic and environmental factors. It is a complex multifactorial disease that is characterized by insulin resistance, diabetes mellitus, various cancers, bone-related disorders, and cardiovascular diseases[2]. One such association is observed in the case of IBD. Adipose tissue also secretes pro- and anti-inflammatory cytokines, among which adipokines are responsible for IBD because of their structural similarity with tumor necrosis factor-alpha (TNF-α), an important cytokine involved in IBD pathogenesis. Leptin and resistin are the major adipokines contributing to IBD[3]. On the basis of fecal calprotectin measurements and intestinal permeability, obesity is also linked to elevated bowel inflammation markers. Nevertheless, epidemiological studies have been unable to consistently link obesity to an increased risk of CD and UC despite these compelling data[4].

Several chemicals, such as dextran sodium sulfate (DSS) and 2,4,6-trinitrobenzene sulfonic acid (TNBS), are known to induce inflammatory bowel disease in rats[5]. Antipsychotic drugs such as olanzapine and sulpiride have been shown to induce obesity in rats[6,7], and a high-fat diet is also a commonly used animal model to study obesity[8]. Microplastics, which are an increasing source of pollutants, have raised concerns about their effects on health. Studies in mice have revealed that microplastics increase the expression of TNF-α and IL-1β, which act as inflammatory mediators and cause damage to the colonic mucosa[9]. Monosodium glutamate, which is widely used as a tastemaker in different foods, is known to cause obesity when it is administered to rats[10]. Studies have also shown that both MSG and microplastic can alter gut bacteria in rats[11]. Hence, the current study utilized both MSG and microplastic, which are administered to rats to mimic obesity-associated IBD, since alterations in gut bacteria are the most characteristic feature of obesity and inflammatory bowel disease[12].

Benincasa hispida (Thunb.) belongs to the Cucurbitaceae family and is commonly known as winter melon, ash gourd, or winter gourd. The most popularly used part of this plant is fruit, which is widely used in Asian countries and is a part of their daily diet. Studies have revealed that the use of fruit as a part of daily consumption is beneficial, as it is one of the rich sources of vitamins such as vitamin C, thiamine, riboflavin, and minerals such as iron and calcium. The pharmacological activities of *Benincasa hispida* have been extensively explored because it is a potential source of a wide variety of essential nutrients. *Benincasa hispida* has been found to have nephroprotective activity and is used to treat epilepsy and other central nervous system (CNS)-related disorders, such as Alzheimer's disease[13]. It is also used as a styptic, antiperiodic, laxative, diuretic, tonic, aphrodisiac, and cardiotonic agent and is also used to treat jaundice, dyspepsia, urinary calculi, blood disease (e.g., hemorrhages from internal organs), insulin, asthma, diabetes, fever, and menstrual disorders and to balance body heat. The seeds of *Benincasa hispida* have been found to have antioxidant activity[14]. Fruit extracts have also been shown to reduce ulcer formation in ulcer-induced rats and mouse models and are known to possess anti-inflammatory activity. The fruit is also said to have hypolipidemic, hypoglycemic, and anorectic effects[15].

Because of the antioxidant, anti-inflammatory, antiulcer, anorectic, and hypolipidemic activities of *Benincasa hispida* fruit, its potential in mitigating obesity associated with IBD can be explored, as an alternative approach for the treatment of obesity associated with IBD is of utmost importance because of increasing incidence rates worldwide. Since *Benincasa hispida* can be easily used in a day-to-day diet, exploring its potential will provide a patient-friendly option for improving health and lifestyle. Obesity and inflammatory bowel disease (IBD) are conditions that have complex multifactorial etiologies; they significantly impact global health, necessitating the development of effective therapeutic strategies. One medicinal plant, Benincasa hispida (Thunb.), has shown promise in terms of diverse pharmacological properties and has potential as a source of bioactive compounds. This study addresses the therapeutic potential of compounds extracted from B. hispida in obesity-associated IBD. Eighteen bioactive compounds were assayed; 11 compounds had drug-likeness properties with adherence to Lipinski's Rule of Five and were therefore identified as potential drug candidates. To further reveal the mechanisms of action of these therapeutics, advanced computational tools and methodologies, including compound–gene set pathway enrichment analysis, network pharmacology, docking studies, and molecular dynamics simulations, have been utilized. Protox safety assessments confirmed the nontoxicity of these compounds, thus further supporting the therapeutic applicability of these drugs. Through Venn diagram analysis of data from the GeneCards and OMIM databases, key proteins associated with obesity and IBD were identified. Pathway enrichment analysis conducted via the DAVID database revealed 810 target proteins across 192 pathways, with 8 pathways directly linked to the pathogenesis of obesity and IBD. Notably, the mechanistic target of rapamycin, MTOR, is an important target for therapy. All the compound, protein, and pathway interactions were visualized via Cytoscape 3.6.1 software as a comprehensive network map. Docking was also carried out via AutoDock 4.2 for the prediction of binding affinities between compounds and MTOR, with Ajmalin presenting the highest binding affinity. Further validation of the interaction stability and efficacy of the Ajmalin-MTOR interaction was conducted through molecular dynamics simulation via the software suite GROMACS 2022.

Hence, the current study was carried out with the aim of evaluating the therapeutic potential of *Benincasa hispida* in ameliorating obesity-associated IBD. Additionally, the molecular mechanisms of the potential

antiobesity and anti-IBD activities of Benincasa hispida have been explored through target identification, compound–gene set enrichment analysis, network pharmacology, and in silico docking.

Materials and methods

Chemicals and reagents

Microplastics were purchased from Haldia Petrochemicals Ltd. (Kolkata, India), and MSG was purchased from a retail shop (supplier: Bakers). All the chemicals used in our study were of analytical grade.

Collection and identification of medicinal plants

The species *Benincasa hispida* thunb. was collected in January from the Hubli region, Karnataka, India. The study plant was identified and authenticated by the Botany Dept. of H.S. Kotambari Science Institute Vidyanagar, Hubballi, Karnataka, India. (Ref no: KLECOPH/2022-23)

Extraction of the plant material

The pulpy part of *Benincasa hispida* fruits were extracted via the Soxhlet extraction method to obtain hydroalcoholic extracts. The apparatus was divided into four different sections: condenser tube, extraction tube, solvent flask, and heating mantle. The sample was inserted into a thimble, which was then inserted into the extraction tube. The solvents used were 70% ethanol and water. The Soxhlet extractor is placed into a flask containing extraction solvent (ethanol and water) and then equipped with a condenser. The solvent was heated to reflux. The solvent vapor travels up the distillation arm and floods into a chamber housing the thimble of solid. The condenser ensures that any solvent cools and drips back into the chamber housing the solid material. The chamber containing the solid material was slowly filled with warm solvent, and some of the desired compounds were dissolved in warm solvent. When the Soxhlet chamber is almost full, the chamber is automatically emptied by a siphon side tube/arm, with the solvent running back down to the distillation flask. This cycle may be repeated many times (hours to days). During each cycle, a portion of the nonvolatile compound dissolves in the solvent, and after many cycles, the desired compound is concentrated in a distillation flask. After extraction, the solvent was removed through a rotary evaporator, yielding the extracted compound. The non–soluble portion of the extracted solid remains thin and is discarded. A rotary evaporator was used to separate the solvents from the water and extracts. The rotary evaporator uses the principle of differences in boiling points to separate the liquid[16].

Liquid chromatography–mass spectrometry (LC–MS)

The hydroalcoholic extract was analyzed via LC-MS (Waters, 2645 Separations Module, Micromass ZQ) to identify putative constituents. Chromatographic separations were performed using a C18 Waters, 50 × 4.6, 5 µm particle size from Thermo Scientific) with a mobile phase of 0.1% formic acid in water (A) and 0.1% formic acid in acetonitrile (B). Initially, the composition is 95.0% A and 5.0% B. This percentage remains the same until 8.00, when the composition changes to 50.0% A and 50.0% B. By 12.00, the composition shifts again to 5.0% A and 95.0% B. This ratio persists at 17.00 and 18.00. Finally, at 20.00, the composition reverts to 95.0% A and 5.0% B. The flow rate, injection volume, and run time were 0.5 mL min − 1, 5 µL, and 20 min, respectively. The LC eluate was directly infused into the mass spectrometer with mass scanning from 0 to 1000 m/z via electrospray ionization in positive and negative modes. The MS parameters were as follows: the capillary voltage was set at 2.8 kV, and the cone voltage was set at 30 V. The source temperature was maintained at 140 °C, with a desolvation temperature of 400 °C and a desolvation gas flow rate of 600 L/Hr. Data processing was carried out via MassLynx V4.1 software[17].

In Silico studies

Drug likeliness and ADMET analysis

The drug-likeness tool DruLito was used to evaluate the drug-like properties of the phytoconstituents identified from the hydroalcoholic extract of *B. hispida* (HABA). These chemicals were further analyzed via the following methods described by Lipinski's rule of five, such as molecular weight, log P, and the number of hydrogen bond donors and acceptors, to check their properties. This analysis provides insight into how similar these phytoconstituents are to drug-like molecules.

The pharmacokinetic properties of the prospective compounds present in the identified phytoconstituents were predicted via the absorption distribution metabolism excretion and toxicity (ADMET) prediction tool ADMETSAR. Computational models have been used to determine 5 key properties, including aqueous solubility, blood–brain barrier permeability, cytochrome P450 inhibition, hepatotoxicity and mutagenicity. These observations provide valuable insights into the general drug-likeness and prospective toxic outcomes of these phytoconstituents. The ADMETSAR results provide significant insights into the nature or risk details of ADME, which will be coupled with these ingredients for future investigations involving the development of candidate neuroprotectants[18].

Mining of phytocompounds and drug-like property prediction

To compile a list of compounds isolated from *Benincasa hispida* (Thunb), herb databases such as IMPPAT[19] and published articles were used. Chemical structural details, such as the molecular weight (MW), molecular formula (MF), number of hydrogen bond donors (NHBD) and acceptors (NHBA), LogP value, BBB SCORE, DLS, MollogP, MollogS, MolpsaA2, MolvolA3, canonical SMILES, and chemical identification number, were sourced from the PubChem chemical database. Using the canonical SMILES, potential drug-like properties were assessed via Lipinski's rule of five models on the MolSoft online server (https://www.molsoft.com/mpr

op/)[20]. Protox (https://tox-new.charite.de/protox_II/) was employed to predict various profiles, including carcinogenicity, hepatotoxicity, nephrotoxicity, and cardiotoxicity, for each compound.

Target identification

Canonical SMILESs were analyzed for target prediction via Swiss target prediction (http://swisstargetprediction.ch/)[21] and STITCH (http://stitch.embl.de/)[22], aligning them with known therapeutic drug molecules. Additionally, target proteins associated with obesity and IBD were pinpointed on the basis of documented obesity and IBD targets sourced from the Gene Cards and Online Mendelian Inheritance in Man (OMIM) Database (https://www.genecards.org/and https://www.omim.org/)[23]. To identify overlapping genes, compound genes and disease genes were merged, and this overlap was visualized via a Venn diagram[24].

Pathway and network analysis

The STRING database (https://string-db.org/) and Kyoto Encyclopedia of Genes and Genomes (KEGG) pathway database (https://www.genome.jp/kegg/) were used to explore protein–protein interactions and molecular pathways influenced by protein targets related to obesity and IBD, respectively. Network connections among compounds, target proteins, and pathways associated with obesity and IBD were visualized via Cytoscape v3.6.1 (https://cytoscape.org/). The network's interpretation was facilitated by using a color scale and node size, which represent the number of edges (edge count) associated with each node. Nodes with the highest edge counts are depicted as large nodes[25].

Ligand and protein preparation

Following the network analysis, compounds exhibiting the highest edge count concerning protein targets were subjected to further investigation for molecular interactions. The 3D structures of each compound were sourced from PubChem (https://pubchem.ncbi.nlm.nih.gov/) in structural data format (.sdf) and transformed into protein data bank format (.pdb) via Discovery Studio Visualizer (https://discover.3ds.com/). Ligand preparation was conducted via Autodock software, which involves the conversion of the .pdb format into (.pdbqt) format for individual ligands, namely, tyrosine, glutamate, ethylβ-d-glucopyranoside, and vitamin C[19].

Protein structures, namely, PIK3CB, PIK3CA, MAPK1, GSK3B, and MTOR, were acquired from the PDB (https://alphafold.ebi.ac.uk/). Each protein's structure was rigorously validated via a Ramachandran plot, ensuring protein qualities of 94.67%, 94.48%, 90.54%, 90.10%, and 100% (https://saves.mbi.ucla.edu/). To facilitate calculations and clean the binding pocket, water molecules and heteroatoms in the protein structure were eliminated via Discovery Studio Visualizer 2019. Individual proteins were prepared for analysis via Autodock software, where the protein (.pdb) format was transformed into (.pdbqt) format. The selection of the chain was based on the completeness of amino acid residues and the presence of the active site region[18,19].

Docking studies

Docking studies were conducted via AutoDock 4.2 (https://autodock.scripps.edu/). The protein structure was refined by adding hydrogen atoms and Kollman charges, and water molecules were eliminated to optimize the macromolecule binding affinity. The grid box was precisely placed at the active site, and the corresponding grid. txt and config.txt files were generated within the designated folder. The AutoDock program was executed by entering the folder's code into the command prompt. The ligand poses exhibiting the highest binding energy with the target protein were subsequently chosen for visualization of ligand–protein interactions in Discovery Studio[26].

Molecular dynamics and simulation

To determine the stability and dynamics of the mTOR protein and its complex with Ajmalin, molecular dynamics (MD) simulations were carried out. The CHARMM36 force field was used for all the simulations in the GROMACS simulation package. Initial structural models of the APO-mTOR and mTOR-Ajmalin complexes were prepared via crystal structures retrieved from the PDB. The ligand topology parameters of Ajmalin were determined with the help of the CGenFF program. Therefore, the parameters are compatible with the CHARMM36 force field. The system was started by solvating the protein and the protein–ligand complex in a cubic box of TIP3P water molecules to maintain at least a 1.0 nm distance between the solute and the boundary of the box. The system was then neutralized via the addition of Na + and Cl- ions, with the ionic strength constant at 0.15 M. To remove all steric clashes and bad contacts, energy minimization was achieved via the steepest descent algorithm. After energy minimization, equilibration was performed in two steps: first, with an NVT ensemble at a constant number of particles, volume, and temperature for the stabilization of the temperature at 310 K by a modified Berendsen thermostat, and then, with an NPT ensemble at a constant number of particles, pressure, and temperature for the stabilization of pressure at 1 bar by the Parrinello–Rahman barostat. Each equilibration phase lasted for 5 nanoseconds, with a time step of 2 femtoseconds. The production MD simulations were carried out with periodic boundary conditions in all directions for 200 ns. The LINCS algorithm was used to restrain all covalent bonds containing a hydrogen atom so that a time step of 2 femtoseconds could be used. The PME method was used for long-range electrostatics with the cutoff of nonbonded interactions at 1.2 nm. All outputs were saved at coordinates, velocities, and values of energies every 10 picoseconds for subsequent analyses. The main analyses included root mean square deviation, root mean square fluctuation, radius of gyration, and solvent accessible surface area. Calculations involving binding free energy were achieved by employing the Molecular Mechanics Poisson–Boltzmann Surface Area (MM–PBSA) methodology available within the g_mmpbsa tool[27].

In vivo studies

Animal housing and maintenance

Wistar albino male rats (18 months) weighing 200–250 g were utilized during experimentation. The animals were housed under a standard 12-hour light and dark cycle and were kept for one week to acclimatize to laboratory conditions before starting the experiment. They were given free access to water and standard feed. These animals were procured from the animal house of K.L.E. College of Pharmacy, Hubballi, Karnataka. The Institutional Animal Ethics Committee (IAEC) reviewed and approved the proposed animal study (Approval No. Mph/NC0221004/KLECoPH/22), as per the guidelines of the Committee for Control and Supervision of Experiments on Animals (CCSEA) in India. All the experimental procedures were conducted in accordance with the ARRIVE guidelines. Furthermore, all the experiments were performed in accordance with relevant guidelines and regulations[28].

Study design

A total of 30 animals were divided into5 groups($n = 6$) each by using block randomization technique to minimize bias and ensure balanced groups. Group I served as normal control, group II was subjected with MSG, and group III, as microplastic-induced group, which were fed a normal chow diet, MSG-induced diet or microplastic-induced diet, respectively. The Group IV rats fed with MSG diet received *Beninscasa hispida* extract (200 mg/kg body weight), and the Group V rats fed with microplastic diet received *Benincasa hispida* extract (200 mg/kg body weight) for 28 days as mentioned in the study timeline.

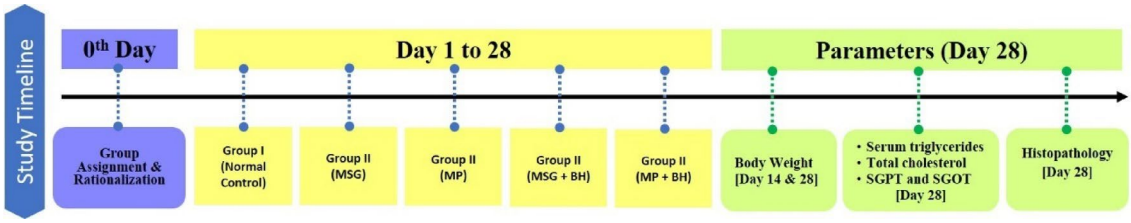

Body weight

The body weights of the rats were measured on days 1, 14 and 28 via a weighing scale.

Biochemical estimation

The animals for the study were subjected to anaesthesia via ketamine and xylazine. Blood samples were collected via retro-orbital sinus puncture, after which the serum was separated from the samples via centrifugation at 3000 rpm for 20 min and stored at 4 °C and analysed within 1 h. The levels of triglycerides (TGs), total cholesterol (TC), SGPT (Serum Glutamate-Pyruvate Transaminase) or alkaline phosphate (ALP), and SGOT (Serum Glutamate-Oxaloacetate Transaminase) or alanine transaminase (ALT) were then measured in the serum samples wherein, TGs was analysed by enzymatic glycerol kinase method, TC by enzymatic cholesterol oxidase method, SGPT and SGOT were analysed by kinetic uv absorbance method, using biochemical analyzer[29].

Fecal matter test

To accurately assess the lipid content in the fecal samples, 1 gram of fecal matter from each cage was ground to a fine powder via a tissue grinder and placed in 25 ml conical tubes. The weight of each tube was recorded, and the samples were subsequently filled with 5 ml of normal saline and mixed thoroughly. Five milliliters of a chloroform: methanol mixture was added and mixed thoroughly to obtain the lipid phase by centrifugation at 1000x g for 10 min at room temperature. The lipid phase was then collected in a glass tube and placed in a fume hood for 3–4 days undisturbed until the whole liquid had evaporated. Finally, the weight of the remaining lipid was taken and subtracted from the initial weight of the fecal matter, providing an accurate assessment of the lipid content in the fecal samples[30].

Histopathological study

The liver and intestine samples from each group were stored in a 10% formalin solution. These samples were subsequently dehydrated with alcohol, cleaned with xylene, and embedded in paraffin. Each sample (5 µm in size) was then stained with hematoxylin and eosin and mounted in neutral dibutylphthalate polystyrene xylene (DPX) media for examination under a light microscope. Then, any tissue abnormalities or changes in the liver or intestine among the different groups were analyzed[31].

Statistical analysis

Each group's mean and standard error of the mean values were computed and the group identifiers were blinded during the data analysis. Repeated-measures ANOVA and Tukey's post hoc test were used to determine whether there were significant differences between the groups. Statistical significance was defined as $p < 0.05$ [32].

S. No	Compound	Molecular Formula	Adduct	RT	Mass	Theoretical Mass
1.	3,10-Dimethoxy-13a-alpha-berbine-2,9-diol	$C_{19}H_{21}NO_4$	M + H	7.12	327.147	327.379
2.	8-Methyl-N-vanillylnonanamide	$C_{18}H_{29}NO_3$	M + H	7.86	307.215	307.432
3.	Galanthamine	$C_{17}H_{21}NO_3$	M + H	9.05	287.152	287.358
4.	Hippeastrine	$C_{17}H_{17}NO_5$	M + H	9.67	315.111	315.324
5.	Tschimganin	$C_{18}H_{24}O_4$	M + H	10.1	287.152	304.385
6.	Andrographolide	$C_{20}H_{30}O_5$	M + H	11.5	350.293	350.453
7.	Dehydroabietylamine	$C_{20}H_{31}N$	M + H	11.7	285.246	285.473
8.	14,15-Dehydro-16-epi-vincamine	$C_{21}H_{24}N_2O_3$	M + H	12.3	352.179	352.433
9.	Marchantin G	$C_{28}H_{22}O_6$	M + H	13.4	454.142	454.477
10.	Moxidectin	$C_{37}H_{53}NO_8$	M + H	13.8	639.337	639.827
11.	Ergocryptinine	$C_{21}H_{27}N_7O_{14}P_2$	M + H	14.6	575.311	663.428
12.	D-(+)-Malic acid	$C_4H_6O_5$	M-H	1.7	134.022	134.087
13.	Ajmalin	$C_{20}H_{26}N_2O_2$	M-H	7.14	326.012	326.438
14.	Atractylenolide III	$C_{15}H_{20}O_3$	M-H	7.84	248.141	248.321
15.	10-Hydroxydecanoate	$C_{10}H_{20}O_3$	M-H	8.69	188.141	188.266
16.	Sebacic acid	$C_{10}H_{18}O_4$	M-H	9.32	202.121	202.249
17.	(E)-9,12,13-trihydroxyoctadec-10-enoic acid	$C_{18}H_{34}O_5$	M-H	10	330.241	330.463
18.	(9E,11E)-13-hydroxyoctadeca-9,11-dienoic acid	$C_{18}H_{32}O_3$	M-H	12.9	296.235	296.449
19.	16-Hydroxypalmitic acid	$C_{16}H_{32}O_3$	M-H	14.9	272.235	272.427

Table 1. LC–MS analysis of the hydroalcoholic extract of *B. hispida* (HABA).

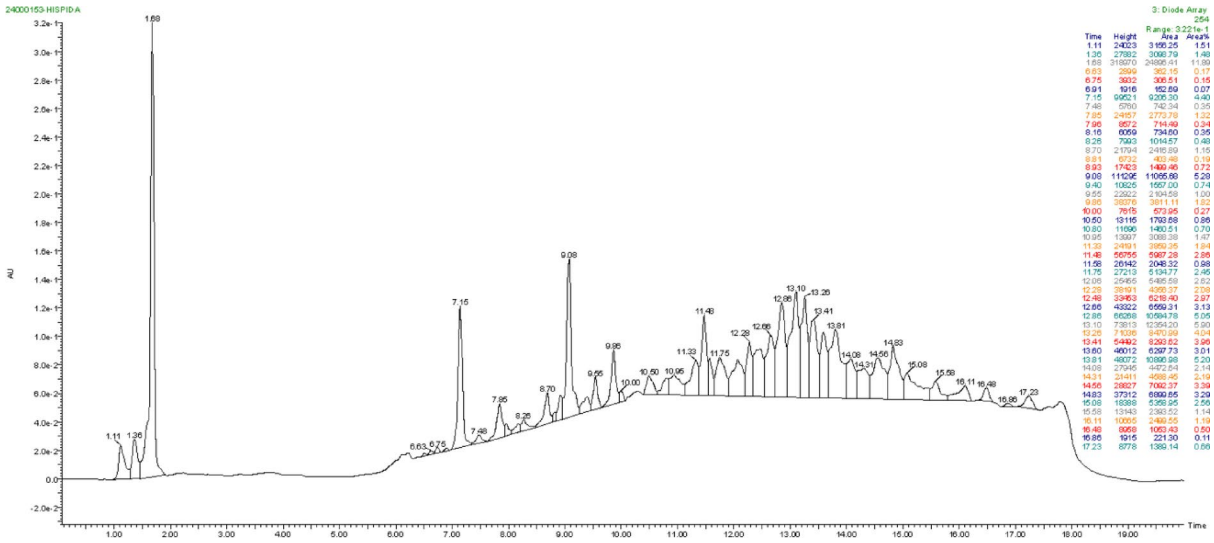

Fig. 1. Chromatogram of the identified phytochemical constituents of HABA via HR-LC–MS.

Results

HR LC–MS analysis of HABA

HR-LC–MS profiling of the hydroalcoholic extract of *B. hispida* (HABA). The percentage yield of HABA was 9.25% w/w; subsequently, the sample was analyzed via HR-LC–MS to determine its phytoconstituents. A total of 19 compounds were identified on the basis of the retention period, experimental m/z values, MS/MS fragments, and discrepancies in the database (NIST library) (Table 1; Fig. 1). Mass spectrometry analysis was performed in positive ionization mode. A major fraction of the MESF mass-charge values (m/z) range from 134 to 639.

Drug likeliness of phytocompounds eluted from HABA

The hydroalcoholic extract of *Benincasa hispida* (HABA) was subjected to HR-LC–MS analysis, leading to the identification of 19 compounds with varying drug-likeness properties. Among these compounds, 14 satisfied Lipinski's rule of five (LRO5), whereas 4 compounds violated it (Table 2). The molecular weights (MWs) of the compounds ranged from 128 to 639.9, with logP values varying from − 6.26 to 5.929, indicating a diverse range of lipophilicities. The AlogP values ranged from − 8.29 to -1.22.

Sr. No.	Title	MW	logp	Alogp	HBA	HBD	TPSA	AMR	nRB	nAtom	LRO5
1	3,10-Dimethoxy-13a-alpha-berbine-29-diol	306	1.004	0.205	5	0	21.7	98.57	2	24	Yes
2	8-Methyl-N-vanillylnonanamide	278	4.503	-0.77	4	0	26.3	85.05	11	22	Yes
3	Galanthamine	268	1.062	-0.56	2	0	21.7	56.62	1	23	Yes
4	Hippeastrine	301	0.352	-0.66	4	0	48	56.18	0	26	Yes
5	Tschimganin	280	4.18	0.8	2	0	35.53	57.89	4	22	Yes
6	Andrographolide	320	2.913	-0.33	5	0	26.3	94	3	25	Yes
7	Dehydroabietylamine	254	5.896	1.22	1	0	0	92.48	2	21	No
8	14,15-Dehydro-16-epi-vincamine	329	1.649	0.879	5	0	32.78	105.6	3	27	Yes
9	Marchantin G	432	3.37	0.942	6	0	35.53	143.9	0	34	Yes
10	Ergocryptinine	639.9	-6.26	-8.29	20	0	183.4	134.6	11	48	No
11	D-(+)-Malic acid	128	-1.47	-1.06	5	0	34.14	24.88	3	9	Yes
12	Ajmalin	300	1.451	-1.31	4	0	6.48	91.61	1	24	Yes
13	Atractylenolide III	228	2.47	1.061	3	0	26.3	67.63	0	18	Yes
14	10-Hydroxydecanoate	168	2.391	-2.67	3	0	17.07	39.43	9	13	Yes
15	Sebacic acid	184	2.282	-2.14	4	0	34.14	41.01	9	14	Yes
16	(E)-9,12,13-trihydroxyoctadec-10-enoic acid	296	3.735	-4.1	5	0	17.07	74.99	15	23	Yes
17	(9E,11E)-13-hydroxyoctadeca-9,11-dienoic acid	264	5.929	-2.07	3	0	17.07	74.92	14	21	No
18	16-Hydroxypalmitic acid	240	5.805	-4.4	3	0	17.07	56.9	15	19	No
19	Moxidextin										

Table 2. Drug-likeness properties of various compounds eluted from HR-LC-MS of HABA.

Notably, compounds such as 3,10-dimethoxy-13a-alpha-berbine-29-diol, galanthamine, and Ajmalin comply with LRO5, making them potential candidates for further pharmacological exploration. On the other hand, compounds such as dehydroabietylamine, ergocryptinine, (9E,11E)-13-hydroxyoctadeca-9,11-dienoic acid, and 16-hydroxypalmitic acid violated LRO5. Dehydroabietylamine violates this rule because of its high logP value of 5.896, suggesting excessive lipophilicity. Ergocryptinine violated LRO5 on multiple fronts: it had a molecular weight of 639.9, which was significantly above the threshold; an AlogP of -8.29; and a TPSA of 183.4, all of which exceeded the limits for drug-likeness. Both (9E,11E)-13-hydroxyoctadeca-9,11-dienoic acid and 16-hydroxypalmitic acid also violated LRO5 due to high logP values of 5.929 and 5.805, respectively, indicating high lipophilicity.

Additionally, most of the compounds presented a low number of hydrogen bond donors (HBDs), with several compounds having zero HBDs and hydrogen bond acceptors (HBAs) ranging between 1 and 20. The topological polar surface area (TPSA) values varied widely, from 0 to 183.4, and the number of rotatable bonds (nRB) ranged from 0 to 15, whereas the number of atoms (nAtom) varied between 9 and 48. This comprehensive analysis of HABA provides valuable insights into the pharmacokinetic properties of these compounds, highlighting their potential as drug candidates and the limitations posed by certain parameters that affect their drug-likeness.

Gene set enrichment and network pharmacology

Figure 2 illustrates the compilation of shared and distinct genes identified among the target, obesity, and IBD groups. Notably, 298 combined genes were discovered to be common across all categories. Intriguingly, the obesity group presented the greatest number of unique genes (5999), followed by the IBD group, with 1866 unique genes. Figure 3 presents the protein-protein interaction map of these protein-coding genes.

Understanding the mechanism of action of phytocompounds from medicinal plants against complex diseases such as obesity and IBD, both in vivo and in vitro, presents significant challenges. In this study, we employed a comprehensive approach involving gene set enrichment analysis, network pharmacology, and docking techniques to elucidate the intricate molecular mechanisms of compounds derived from *Benincasa hispida* (Thunb). The identification of phytocompounds within *Benincasa hispida* (Thunb.) was carried out through extensive searches of herb databases and the literature, resulting in the identification of 18 compounds. The selection criteria for these compounds encompassed essential factors such as oral bioavailability, half-life, and drug similarity, which are crucial for gene set enrichment and network pharmacology analyses. Among the 18 compounds, 11 exhibited positive drug similarity scores, indicating their potential therapeutic relevance. All 11 phytoconstituents were found to adhere to the Rule of Five, a set of guidelines established by Christopher A. Lipinski, which are commonly used in drug discovery and medicinal chemistry. This rule assists in evaluating a compound's potential success as an orally active drug by assessing its pharmacokinetic and physicochemical properties. The criteria, including a molecular weight of 500 g/mol or less, 5 or fewer hydrogen bond donor sites, a logP (partition coefficient) of 5 or less, and 10 or fewer hydrogen bond acceptors, were met by these compounds. While the rule of five provides valuable guidance, it is not an absolute rule, and other factors also influence a compound's pharmacokinetic behavior and drug-like properties.

Furthermore, pathway enrichment analysis was performed for 810 targets via STRING and the KEGG pathway database. This analysis revealed 810 targets associated with 192 distinct pathways. Upon interpretation, 8 pathways were directly linked to the pathogenesis of obesity and IBD. Among these targets, MTOR was

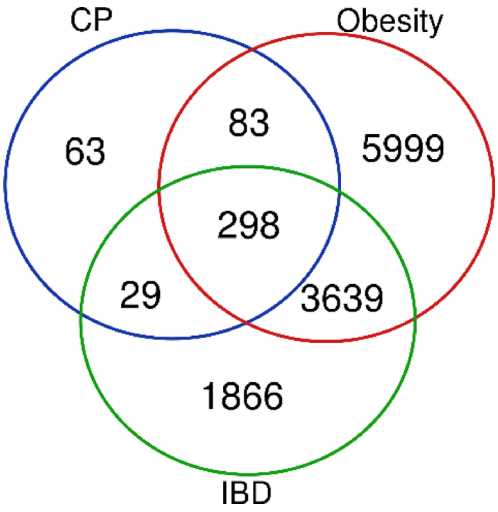

Fig. 2. Venn diagram of obesity and IBD.

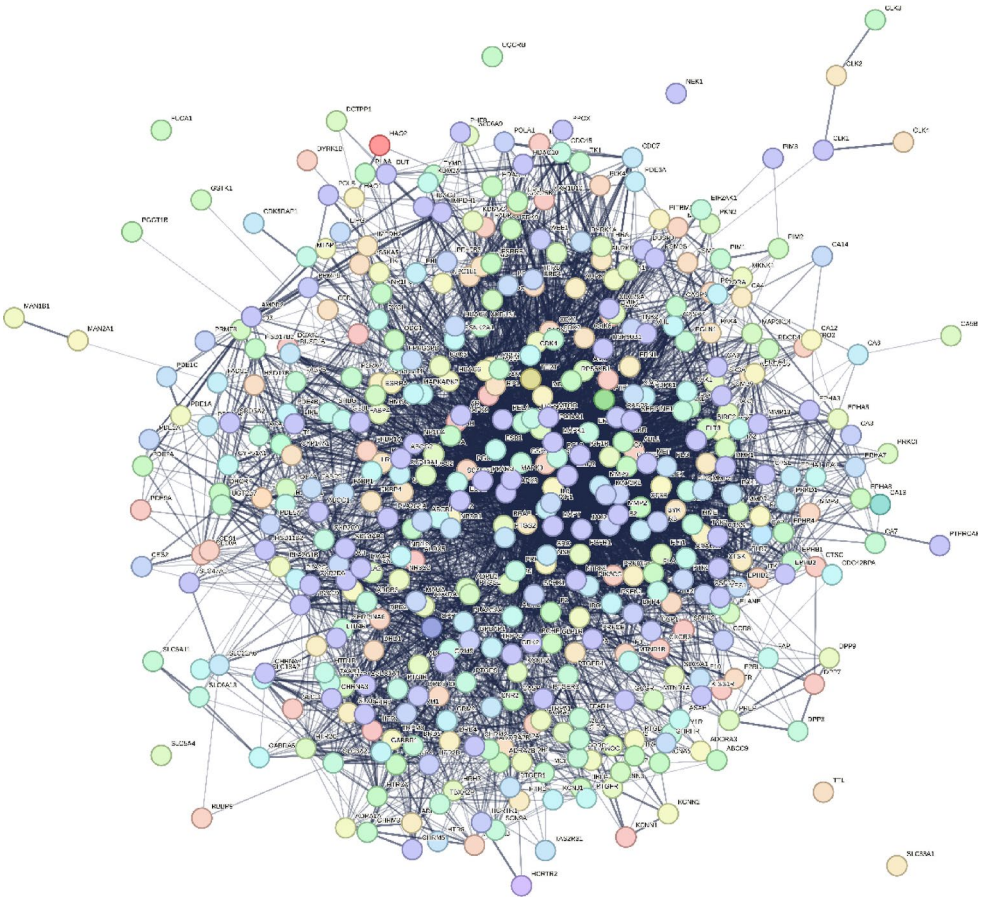

Fig. 3. Probable protein–protein interaction network[33].

identified as a therapeutic target for obesity and IBD (Fig. 4). Notably, among the 2 compounds, Ajmalin and dihydrocapsaicin targeted these MTOR proteins. Moreover, these targets are involved in pathways such as the PI3K-Akt signaling pathway, insulin signaling pathway, mTOR signaling pathway, AMPK signaling pathway and adipocytokine signaling pathway. These pathways were identified as crucial in the context of obesity and IBD (Table 3)[34–36].

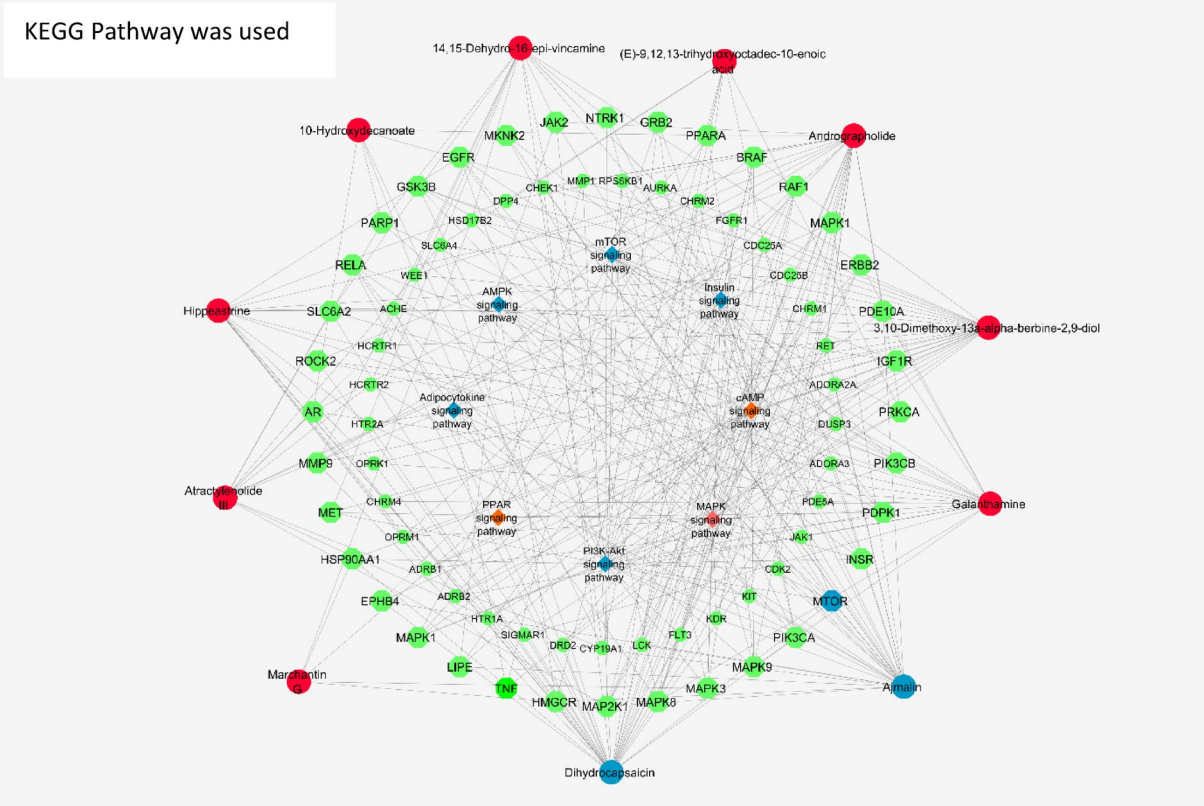

Fig. 4. Network representation of compounds, proteins, and pathway interactions[33].

Pathway	Genes within pathway
cAMP signaling pathway	MAPK1 LIPE PTGER2 CREBBP MAPK3 PIK3CA PAK1 HTR6 MAP2K1 ADRB2 DRD5 CHRM1 HTR1A ROCK2 HTR1F PDE4B PTGER3 NPY1R DRD2 PDE10A ADORA1 ADRB1 GLP1R HTR1D GABBR1 PDE4A DRD1 MAPK8 ROCK1 RELA PPARA MAPK9 CHRM2 RAF1 BRAF GIPR ADORA2A PIK3CB
PI3K-Akt signaling pathway	MAPK1 RPS6KB1 FLT3 CDK4 MDM2 PDGFRB MAPK3 KDR PIK3CA CDK6 CDK2 ERBB2 EGFR FLT1 CSF1R KIT HSP90B1 MAP2K1 INSR CHRM1 MET GSK3B HSP90AA1 PTK2 PDPK1 EPHA2 MTOR SGK1 MCL1 PKN2 HSP90AB1 SYK JAK2 GRB2 BCL2 RELA IL6 FGFR1 CHRM2 RAF1 PRKCA PIK3CG NTRK1 JAK3 IGF1R JAK1 PIK3CB
MAPK signaling pathway	MAPK1 DUSP3 MAPK14 FLT3 CDC25B MKNK2 PDGFRB MAPK3 KDR ERBB2 EGFR PAK1 FLT1 CSF1R KIT DUSP16 MAP2K1 INSR CASP3 MET MAPT EPHA2 MAPKAPK2 PLA2G4A GRB2 MAPK8 RELA FGFR1 MAPK9 PLA2G4B TNF RAF1 PRKCA BRAF NTRK1 RPS6KA5 MAP3K14 IGF1R MKNK1
Insulin signaling pathway	MAPK1 PYGL GCK RPS6KB1 LIPE MKNK2 MAPK3 PIK3CA PRKCI MAP2K1 INSR GSK3B ACACB PDPK1 MTOR PTPN1 GRB2 MAPK8 MAPK9 RAF1 BRAF MKNK1 PIK3CB
mTOR signaling pathway	MAPK1 RPS6KB1 MAPK3 PIK3CA MAP2K1 INSR GSK3B PDPK1 MTOR SGK1 GRB2 TNF RAF1 PRKCA BRAF IGF1R PIK3CB
PPAR signaling pathway	FABP4 FABP2 PPARG FABP1 FABP5 PPARD MMP1 PDPK1 FABP3 ILK PPARA NR1H3
AMPK signaling pathway	RPS6KB1 LIPE PIK3CA PPARG HMGCR INSR ACACB PDPK1 MTOR ADRA1A PFKFB3 IGF1R PIK3CB
Adipocytokine signaling pathway	ACACB MTOR JAK2 MAPK8 RELA PPARA MAPK9 TNF

Table 3. Pathways associated with obesity and IBD progression modulated by phytocompounds.

Docking studies

Molecular docking studies involving the interactions of various compounds with specific protein targets were conducted via enrichment analysis. The interaction of the mTOR protein with various ligands—Ajmalin, dihydrocapsaicin, and orlistat—was studied to determine the binding affinities and identify key protein-ligand interactions. Ajmalin exhibited the highest binding affinity for mTOR, with a binding energy of -7.8 kcal/mol. The primary interactions involved residues HIS1670, ASN1703, MET1704, HIS1716, SER1707, and LEU1685 (Fig. 5). Dihydrocapsaicin displayed a lower binding affinity of -5.8 kcal/mol, interacting mainly with residues HIS2289, GLN312, LYS313, GLN1722, ILE2267, and ASN292 (Fig. 6). Orlistat had the lowest binding affinity of -5.2 kcal/mol, interacting with residues ILE2263, ILE2267, HIS1719, THR1723, ASN292, GLN1726, and ARG270 (Fig. 7). These findings suggest that Ajmalin has the strongest interaction with the mTOR protein among the three ligands, indicating its potential as a more effective modulator of mTOR activity. These interactions were further characterized by assessing changes in ligand orientation after docking and identifying hydrogen bond

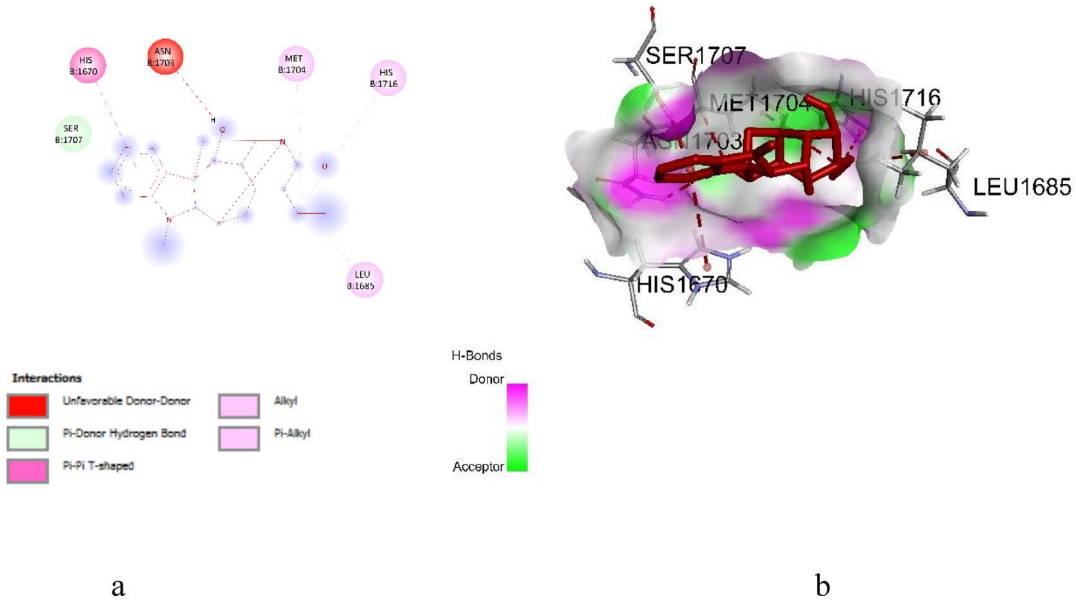

Fig. 5. Interaction of Ajmalin with MTOR: (**a**) 2D representation and (**b**) 3D representation.

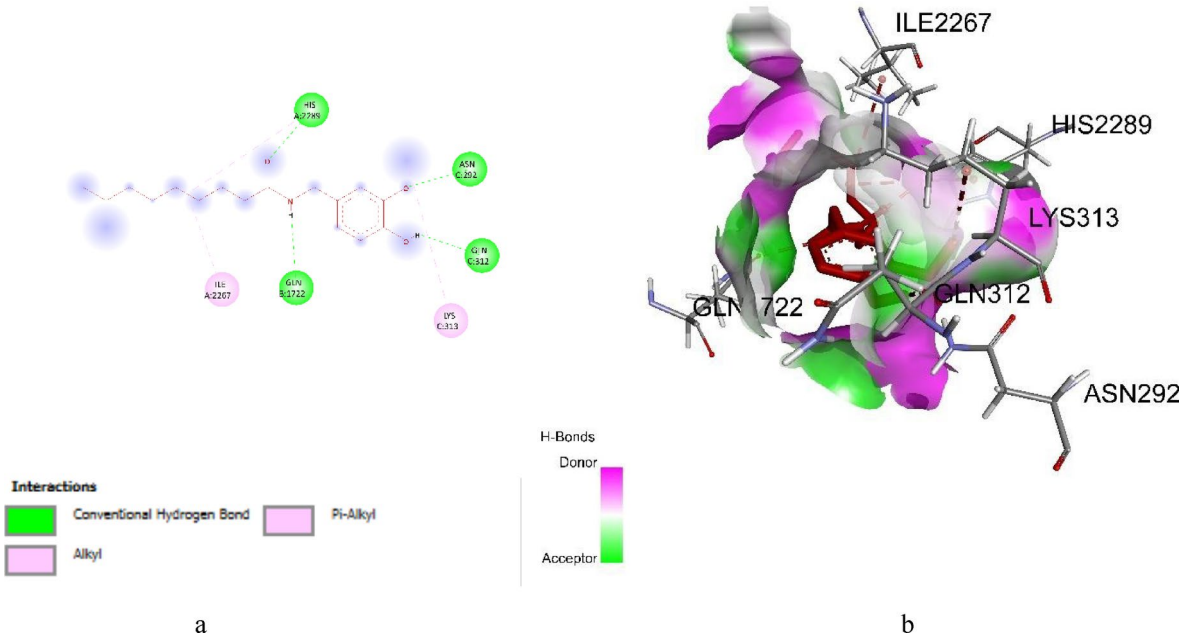

Fig. 6. Interaction of dihydrocapsaicin with MTOR: (**a**) 2D representation (**b**) 3D representation.

interactions. Detailed information can be found in Table 4, summarizing the binding energies and the molecular interactions of these compounds with their respective protein targets.

Molecular dynamics and simulation

We generated trajectories for both the protein APO-MTOR and the protein-ligand complex, which included the protein MTOR and the ligand Ajmalin. These trajectories were used in MDS analysis, such as the calculation of parameters such as RMSD, RMSF, SASA and radius of gyration. The outcome of this kind of analysis quantitatively describes the degree of deviation and fluctuations across these kinds of parameters, which might provide insights into the behavior of the system.

The RMSD plot of the complex with the protein is plotted for a period of 200 ns. The RMSD fluctuated up to 75 ns and then stabilized throughout the simulation duration. The stability of the RMSD indicates the stable configuration of the ligand when it is subjected to dynamics in the system (Fig. 8). This means that the deviation up to 75 ns is a level of conformational change in the protein-ligand complex during the course of the MD

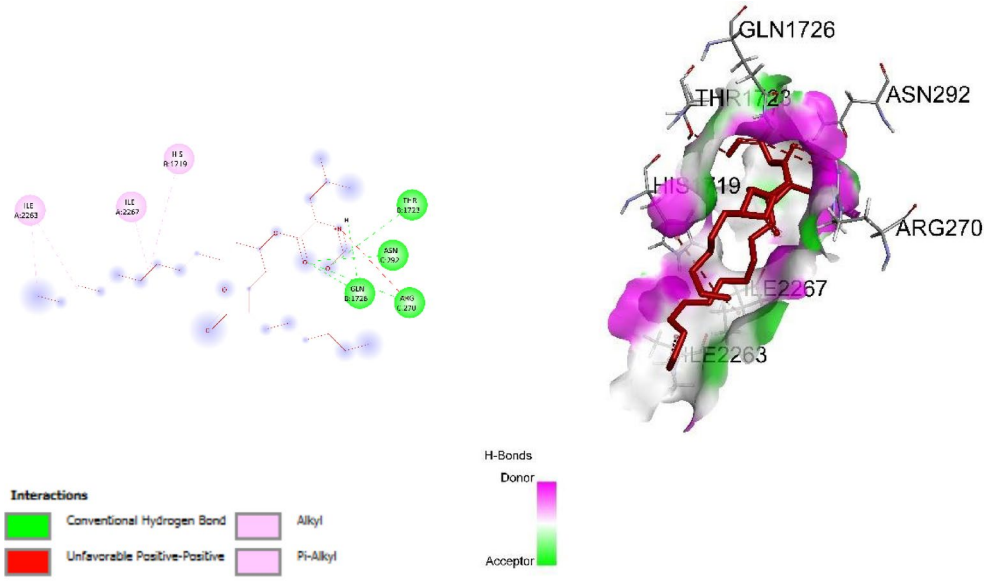

a b

Fig. 7. Interaction of orlistat with MTOR (**a**) 2D representation (**b**) 3D representation.

Protein–ligand receptor	Binding affinity	Protein–ligand interaction
MTOR- Ajmalin	− 7.8	HIS1670, ASN1703, MET1704, HIS1716, SER1707, LEU1685
MTOR- Dihydrocapsaicin	− 5.8	HIS2289, GLN312, LYS313, GLN1722, ILE2267, ASN292
MTOR- Orlistat	− 5.2	ILE2263, ILE2267, HIS1719, THR1723, ASN292, GLN1726,ARG270

Table 4. Binding affinities, hydrogen bond interactions and nonhydrogen bond interactions of the compounds with their protein targets.

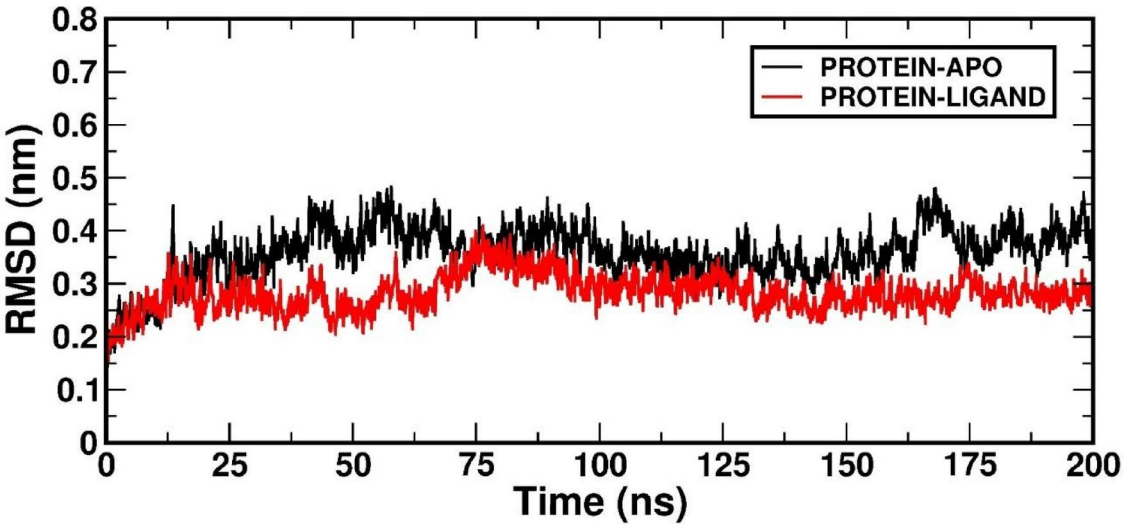

Fig. 8. RMSD plot of APO and the protein–ligand complex for a duration of 200 ns.

simulation. The lower the RMSD value fluctuations (in nm) are, the better the stability in the dynamics of the system.

We subsequently performed root mean square fluctuation (RMSF) analysis to assess the loss of stability in various regions. The RMSF plot analysis for the MTOR protein bound to Ajmalin is shown in Fig. 9. Higher values of RMSF depict flexible regions, and a region with low RMSF shows that the dynamics are restrained. In

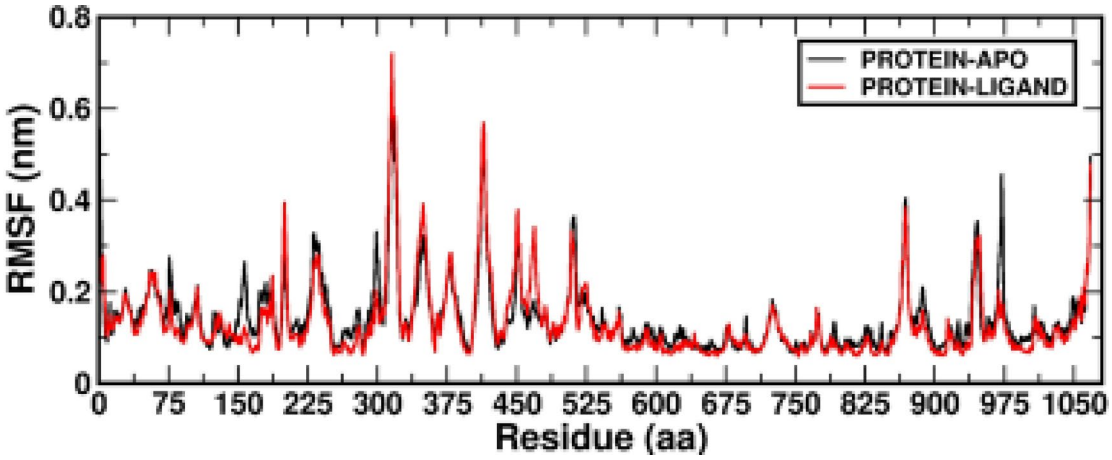

Fig. 9. RMSF plot of APOs and protein–ligand complexes for a duration of 200 ns.

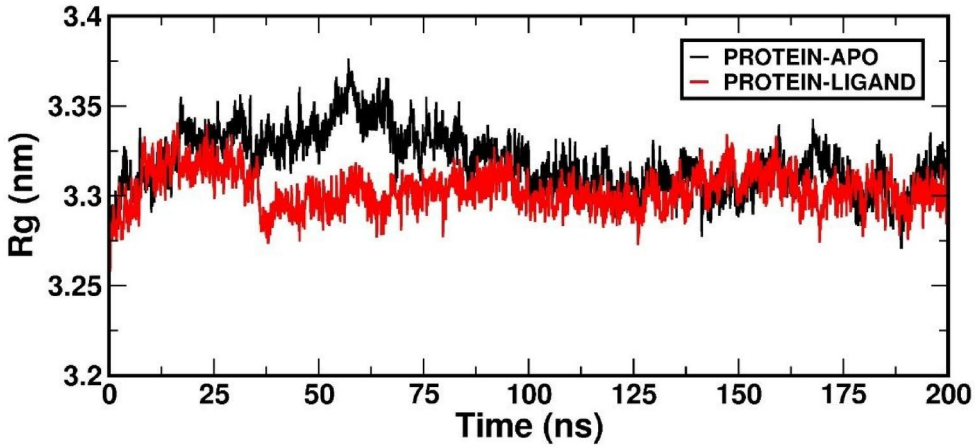

Fig. 10. Radius of gyration plot of APOs and protein–ligand complexes for a duration of 200 ns.

fact, the analysis confirmed that Ajmalin binds to the protein tightly and in a very stable manner, with negligible disturbances in the protein itself.

The Rg plot clearly revealed the compactness of the protein structure. Greater fluctuations throughout the simulation result in structural instability. In this investigation, the values for the Rg plot are constantly ~ ~ 1.45 nm, indicating that for the system for the duration of the 200 ns simulation time, the Ajmalin ligand is very compact and stable (Fig. 10).

We analyzed the solvent-accessible surface area plot for the protein–ligand complex over a simulation period of 200 ns. The SASA is essentially the surface area of a protein that is accessible to a solvent and often becomes a predictor of stability. This profile was shown to be persistent with no fluctuations in the accessible area of the solvent throughout this duration, as the values were within ~ 500 nm^2 and constant values are shown in the plot given in Fig. 11.

We carried out molecular dynamics (MD) simulations and analyzed them via the MMPBSA method. The results indicate that the total binding energy of the system was consistently bound throughout the simulation duration, with an average value of approximately – 16.596 +/- 11.889 kJ/mol. In addition, the total van der Waals energy of the system was calculated to be -85.72 +/- 8.983 kJ/mol.

Effects of MSG and microplastic intake on body weight

During the experimental study, the body weights of the rats were measured on days 1, 14, and 28. On day 14, the body weights of the rats in the MSG group were significantly greater than those of the normal group ($p < 0.01$). On the other hand, compared with those in the normal group, the body weights of the rats in the microplastic-treated groups were significantly lower on day 14 ($p < 0.05$), and the extract-treated groups presented a protective effect, as depicted in Fig. 12. On day 28, the MSG-treated group presented a significant increase in body weight compared with the normal group ($p < 0.001$), and the MP group presented a significant decrease in body weight compared with the normal group ($p < 0.01$), as shown in Fig. 13.

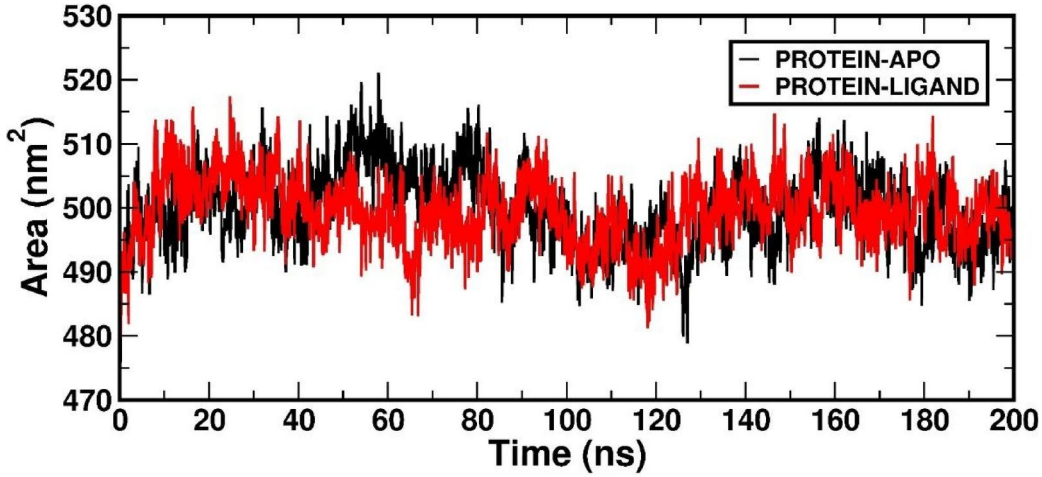

Fig. 11. SASA plot of APO and the protein-ligand complex for a duration of 200 ns.

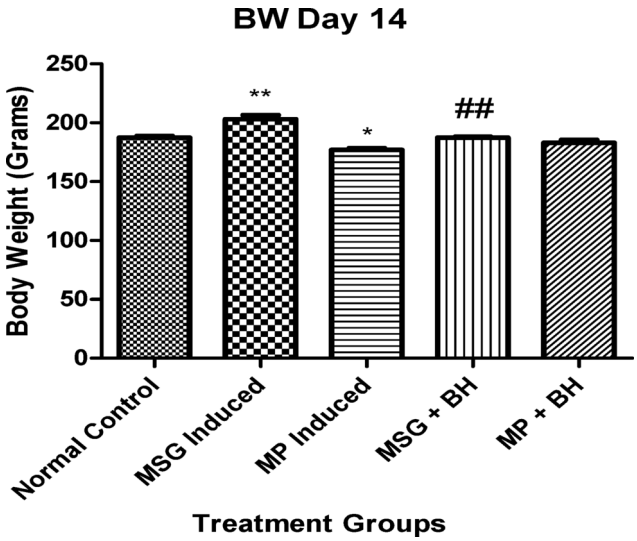

Fig. 12. Effects of *B. hispida* on the body weight of Wistar rats on day 14. Mean ± SEM ($N = 3$): one-way ANOVA with Tukey's multiple comparison test, where $^{**}p < 0.01$ compared with normal, $^{*}p < 0.05$ compared with normal and $\#\#p < 0.01$ compared with MSG-induced samples.

Estimation of biochemical parameters

SGPT/ALT, SGOT/AST, TC and TG are commonly used as liver function biomarkers. On day 28, the triglyceride and total cholesterol levels were significantly greater in the MSG and MP groups than in the normal group ($p < 0.001$), and the extract-treated groups presented protective effects, as depicted in Figs. 14 and 15, respectively. On the other hand, the MSG-treated group presented a significant decrease in the SGPT, and the MP-treated group presented a significant increase in the SGPT compared with the normal group ($p < 0.001$), as shown in Fig. 16. The SGOT scores were significantly lower in the MSG and MP groups than in the normal group ($p < 0.001$), as shown in Fig. 17.

Fecal matter analysis

After 28 days, the lipid content in the groups treated with MSG and MP was greater than that in the other groups. The normal control group had a lipid content of 0.62 g. The MSG- and microplastic-treated groups presented lipid contents of 10.5 g and 16.7 g, respectively. The extract-treated MSG group presented a lower lipid content: MSG + BH (5.6 g). Similarly, the lipid content of the extract-treated microplastic group was lower than that of the MP + BH group (6.2 g). Figure 18 shows the results obtained after centrifuging feces suspended in chloroform: methanol. The centrifugation process led to the separation of three distinct layers. Phase '1' corresponds to the aqueous phase, Phase '2' contains insoluble components, and Phase '3' consists of the extracted lipids.

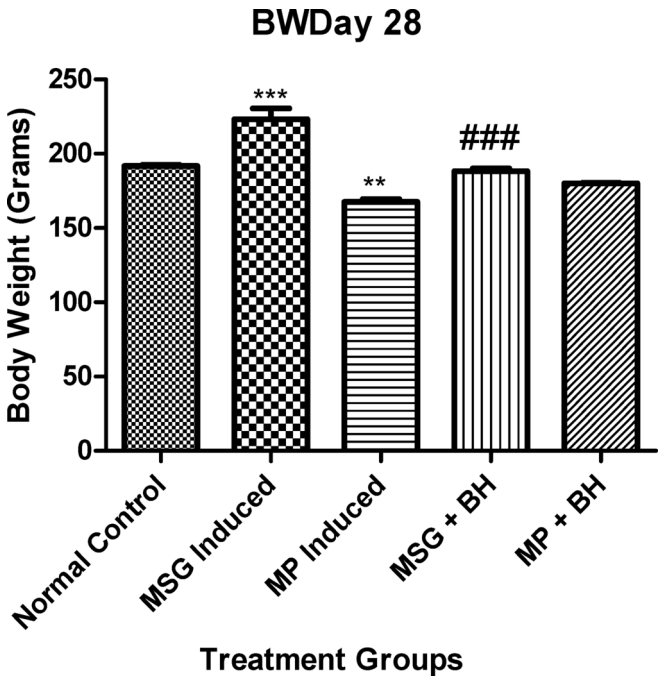

Fig. 13. Effects of *B. hispida* on body weight on day 28 in Wistar rats. Mean + SEM ($N = 3$): Examination via one-way ANOVA (Tukey multiple comparison test), where ***$p < 0.001$ compared with normal controls, **$p < 0.01$ compared with normal controls and ###$p < 0.001$ compared with MSG-induced MS.

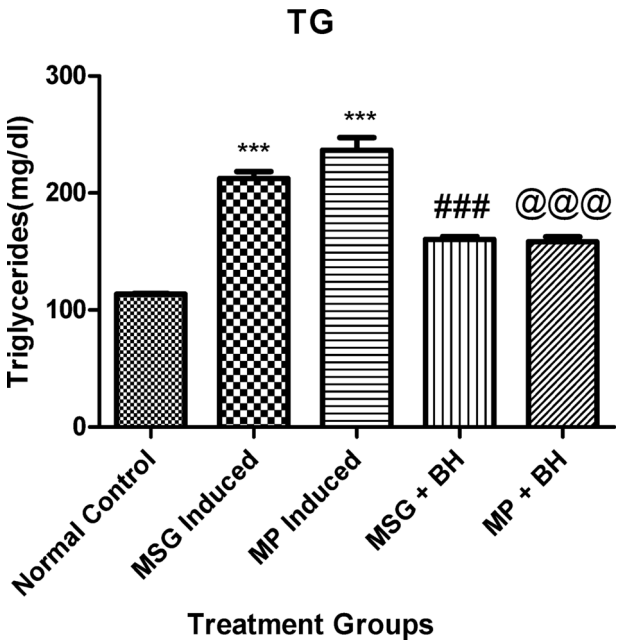

Fig. 14. Effects of *B. Hispida* on TG levels on day 28 in Wistar rats, mean + SEM ($N = 3$): one-way ANOVA with Tukey's multiple comparison test, where ***$p < 0.001$ compared with normal, ###$p < 0.001$ compared with MSG-induced and @@@$p < 0.001$ compared with MP-induced.

Histopathological examination of the liver

Group I control

In the control group, the liver tissue appeared healthy, with no visible signs of damage or abnormal changes. The sinusoids, which are small blood vessels in the liver, appeared clear, with no congestion or blood flow issues. The central veins did not show any swelling or blood pooling, suggesting normal venous circulation. There were no signs of immune cell infiltration, which typically indicates an inflammatory response in the liver. There are no

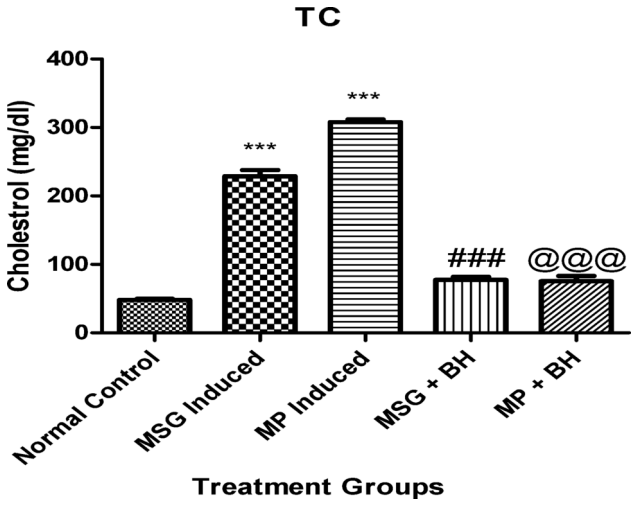

Fig. 15. Effects of *B. hispida* on TC levels in Wistar rats on day 28. Mean ± SEM ($N = 3$): one-way ANOVA (Tukey's multiple comparison test), where $^{***}p < 0.001$ compared with normal, $^{###}p < 0.001$ compared with MSG-induced and $^{@@@}p < 0.001$ compared with MP-induced.

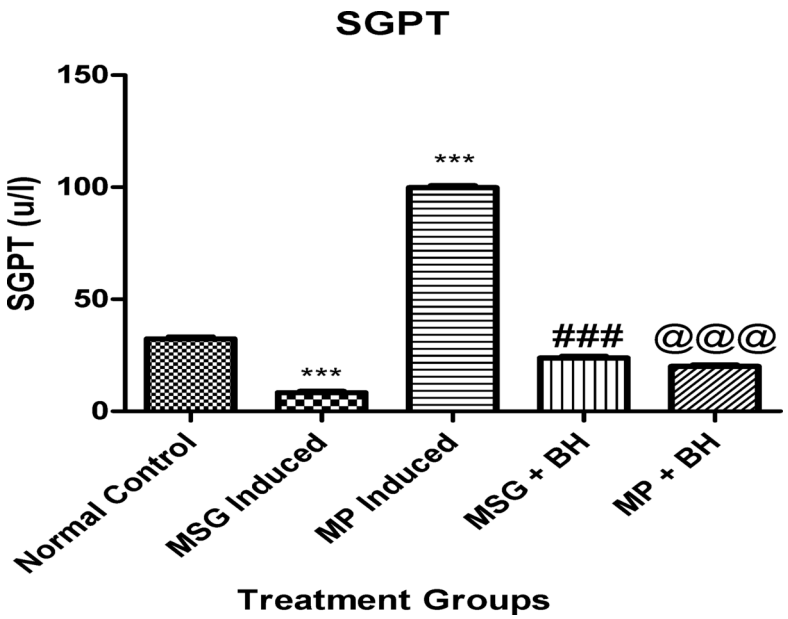

Fig. 16. Effects of *B. hispida* on SGPT levels on day 28 in Wistar rats. Mean ± SEM ($N = 3$): one-way ANOVA (Tukey's multiple comparison test), where $^{***}p < 0.001$ compared with normal controls, $^{###}p < 0.001$ compared with MSG-induced patients and $^{@@@}p < 0.001$ compared with MP-induced patients.

signs of lipid accumulation in liver cells, which is often associated with metabolic disturbances or toxicity. Liver cells (hepatocytes) appeared normal without any swelling as depicted in Fig. 19(A), which is a key indicator of cellular injury.

Group II MSGs Induced

In the MSG-induced group, the liver tissue exhibited venous and sinusoidal congestion. There was noticeable congestion in both the veins and sinusoids. Venous congestion refers to the swelling or pooling of blood in the liver's central veins, whereas sinusoidal congestion refers to blood buildup in the smaller capillaries (sinusoids). These changes were accompanied by moderate fatty acid changes and mild inflammation, as shown in Fig. 19 (B). There were mild signs of inflammation, with the presence of immune cells. These findings suggest that the liver was undergoing an inflammatory response, likely due to MSG-induced injury.

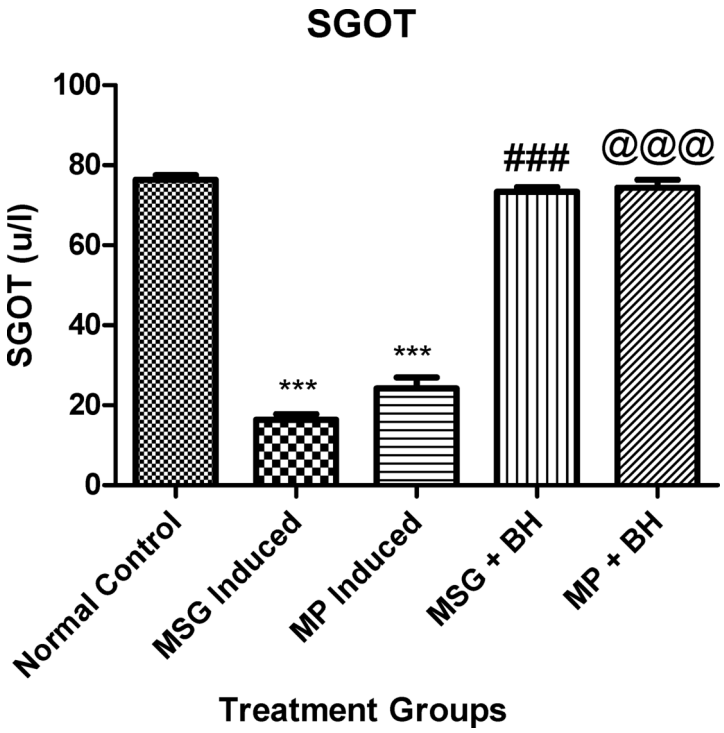

Fig. 17. Effects of *B. Hispida* on SGOT levels on day 28 in Wistar rats, as determined by one-way ANOVA ($N = 3$): Tukey's multiple comparison test, where ***$p < 0.001$ compared with normal controls, ###$p < 0.001$ compared with MSG-induced and @@@$p < 0.001$ compared with MP-induced rats.

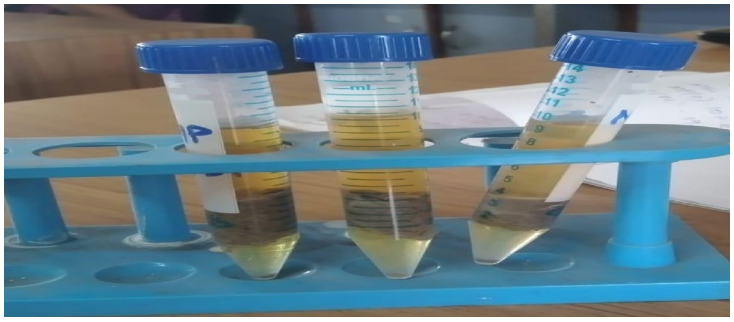

Fig. 18. Sample of dissolved feces after centrifugation.

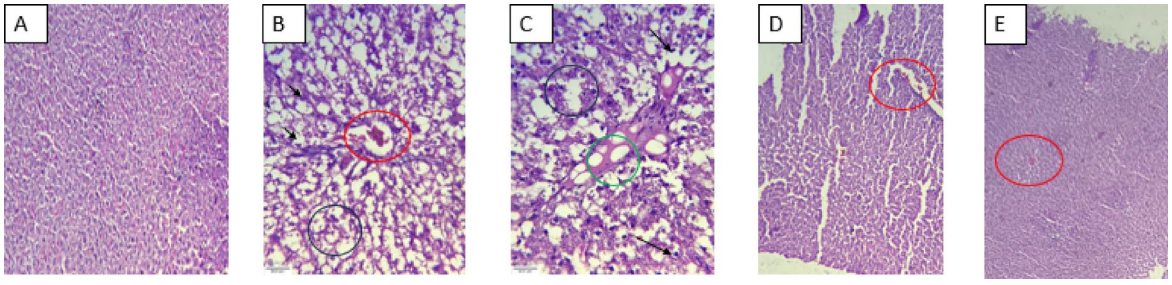

Fig. 19. Histopathology of centrilobular section of the rat liver with H&E staining: (**A**) normal 10X, (**B**) MSG group 40X, (**C**) MP group 40X, (**D**) MSG + BH group 10X, (**E**) MP + BH group 4X, black ring-sinusoidal congestion, red ring-venous congestion, black arrow-inflammatory cells, and green ring-balloon degeneration.

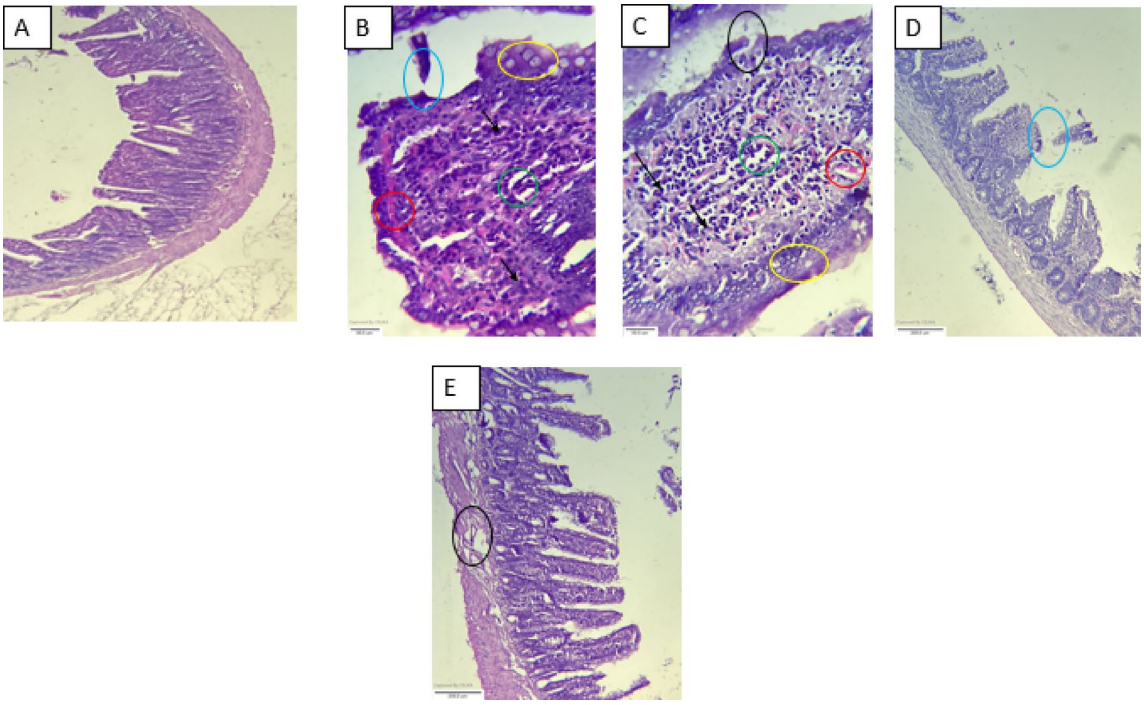

Fig. 20. Histopathology of a rat intestine specifically colon sections were selected and stained with H&E: (**A**) normal group 10X, (**B**) MSG group 40X, (**C**) MP group 40X, (**D**) MSG + BH group 10X, (**E**) MP + BH group 10X, black ring-epithelial exfoliation, red ring-congestion, black arrow-inflammatory cells, green ring-edema, blue ring-vilous destruction and yellow ring-ulceration.

Group III Microplastic (MP) Induced

Compared with that from the MSG group, the liver tissue from the microplastic-induced group presented even more severe damage. The central veins exhibited venous congestion with significant blood pooling, a sign of impaired venous return. These findings indicate that MPs have a strong effect on the ability of the liver to manage blood circulation. In addition to venous congestion, sinusoids also presented moderate congestion, indicating that blood flow throughout the liver was impaired at multiple levels. There was severe balloon degeneration with marked swelling of the hepatocytes, reflecting a high degree of cellular injury as depicted in Fig. 19 (C). This is a serious sign of liver dysfunction. The liver showed moderate fatty infiltration, a common sign of metabolic stress or toxicity. These findings suggest that MP treatment might have caused lipid metabolism issues in the liver. Mild inflammatory changes were noted, indicating that the liver was undergoing some degree of immune response, likely in response to the damage caused by MP.

Group IV (MSG + BH) and Group V (MP + BH) (treatment group)

Compared with those from the MSG and MP groups, the liver tissue from the treatment groups presented an intermediate level of damage. There was moderate congestion in the veins. This finding indicates that while some blood flow disruption occurred, it was not as severe as it was in the MSG or MP groups. Unlike the MSG and MP groups, the treatment groups did not show any signs of inflammation. These findings suggest that the treatment may have helped reduce the immune response and prevented further liver damage. There was no sign of fatty infiltration in the liver cells, which could suggest that the treatment helped prevent lipid accumulation or that liver function was maintained (Figures D &E).

Histopathological examination of the intestine

Group I normal control

The intestinal tissue of the control group appeared healthy and intact, with no significant abnormalities. There were no signs of blood flow disruption in the blood vessels of the intestine. The vasculature appeared normal, with no pooling of blood or congestion. No excessive fluid accumulation was observed in the intestinal tissue, indicating that there was no abnormal swelling or tissue damage due to fluid retention. The tissue showed no signs of an immune response, such as infiltration by immune cells or other inflammatory markers. The villi (finger-like projections in the intestines that increase the surface area for nutrient absorption) were intact, with no signs of structural damage or atrophy. The epithelial cells lining the intestines were normal, with no evidence of sloughing or detachment of these cells from the underlying tissue. There were no lesions or ulcers present in the mucosal layer, indicating that the intestinal lining was healthy and intact (Fig. 20A).

Group II MSGs Induced

In the MSG-treated group, there were several signs of intestinal damage and disruption. The most prominent feature was inflammation, characterized by the presence of immune cells (such as neutrophils and macrophages) infiltrating the intestinal tissue. These findings suggest that MSG exposure triggers an immune response, likely due to irritation or damage caused by the substance. The blood vessels in the intestinal tissue showed moderate congestion, indicating that blood flow was somewhat impaired, with some pooling or swelling in the capillaries and veins. The villi presented moderate damage, such as flattening or shedding of the villous structures. This would impact the surface area available for nutrient absorption and could result in compromised intestinal function. Mild edema, or fluid retention in the tissue, was present. This finding indicates that there was some degree of swelling due to increased permeability in the blood vessels or the inflammatory response. Mild ulceration was observed, with small lesions or breaks in the mucosal lining, as depicted in Fig. 20 (B). These findings suggest that MSG exposure causes damage to the protective intestinal lining, resulting in some localized tissue injury.

Group III Microplastic (MP) Induced

The MP-treated group presented even more severe damage to the intestinal tissue. The blood vessels within the intestine exhibited severe congestion, indicating significant pooling of blood and severe disruption of blood flow and vascular dysfunction. The inflammation in the MP group was more pronounced, with a greater number of immune cells infiltrating the tissue. These findings suggest that, compared with MSG, MP causes a more intense inflammatory response. The intestinal epithelium exhibited signs of exfoliation, where cells detached from the tissue, indicating cellular damage and injury to the protective lining. Larger or deeper ulcers were observed, indicating more severe mucosal damage and potential disruption of the intestinal barrier. Like in the MSG group, mild edema was observed, suggesting that fluid accumulation in the tissue was a common feature of intestinal injury induced by both the MSG and the MP, as shown in Fig. 20 (C).

Group IV (MSG + BH) and Group V (MP + BH) (treatment groups)

The treatment groups presented some degree of intestinal damage, although the damage was not as severe as that in the MSG and MP groups. The blood vessels within the intestines exhibited moderate congestion, which was not as pronounced as that in the MSG and MP groups. This suggests that while there was some disruption in blood flow, it was less severe. Inflammation was generally mild or absent in the treatment groups. This finding could indicate that the treatment helped mitigate the inflammatory response caused by MSG or MP or that it may have prevented the inflammatory cascade from becoming severe. Some instances of villous destruction were noted, suggesting that the treatment was not entirely protective against damage to the villi. However, the level of damage was moderate, and in some cases, the villi appeared relatively intact. There were instances of epithelial exfoliation in the treatment groups, but these were less frequent and less severe than they were in the MSG and MP groups. These findings suggest that the treatment might have helped maintain the integrity of the intestinal epithelium to some extent. No significant ulcerations were observed, suggesting that the treatment helped prevent the development of more severe mucosal lesions or damage, as illustrated in Fig. 20 (D) and Figure (E).

Discussion

This research identified 19 compounds from *Benincasa hispida*, among which 11 had positive drug similarity scores. Crucially, all 11 phytoconstituents, 3,10-dimethoxy-13a-alpha-berbine-29-diol, dihydrocapsaicin, galanthamine, hippeastrine, andrographolide, 14,15-dehydro-16-epi-vincamine, marchin G, Ajmalin, atractylenolide III, 10-hydroxydecanoate and (E)-9,12,13-trihydroxyoctadec-10-enoic acid, adhered to Lipinski's Rule of Five, indicating their potential as orally active drugs. This compliance is pivotal in drug discovery, ensuring that compounds with favorable pharmacokinetic and physicochemical properties are more likely to be effective and safe for use. The safety of these compounds was also evaluated via TOX prediction. TOX prediction provides toxicity predictions on the basis of the entered data. This may include predictions related to acute toxicity, mutagenicity, carcinogenicity, reproductive toxicity, etc. The results are typically presented in the form of numerical values, charts, or qualitative assessments. Several compounds, including 3,10-dimethoxy-13a-alpha-berbine-29-diol, dihydrocapsaicin, galanthamine, hyperkin, andrographolide, 14,15-dehydro-16-epi-vincamine, marchin G, ergocryptinine, D-(+)-malic acid, Ajmalin, atractylenolide III, 10-hydroxydecanoate, (E)-9,12,13-trihydroxyoctadec-10-enoic acid, (9E,11E)-13-hydroxyoctadeca-9,11-dienoic acid and 16-hydroxypalmitic acid, exhibited nontoxic properties, as they did not violate essential toxicity factors such as hepatotoxicity, carcinogenicity, immunotoxicity, mutagenicity, or cytotoxicity. This safety profile is crucial when these compounds are considered for therapeutic applications[37]. Ajmalin and dihydrocapsaicin are essential nutrients that play several important roles in the body, including their potential impact on inflammatory bowel disease (IBD) and obesity management. Additionally, pathway enrichment analysis via STRING and the KEGG pathway database identified 810 targets across 192 distinct pathways. A detailed analysis revealed that 8 pathways were directly associated with the pathogenesis of obesity and IBD. Among these pathways, targets such as MTOR are common therapeutic targets for obesity and IBD[38,39]. This information provides a comprehensive understanding of the molecular pathways relevant to these diseases.

The results of the molecular docking studies provided further insights into the interactions between specific compounds, Ajmalin and dihydrocapsaicin, and the standard drug oralistat, the identified therapeutic target MTOR. The observed binding energies and interactions in these studies offer valuable information about the potential effectiveness of these compounds in modulating the activity of these targets[40]. Implications for Obesity and IBD: The results of this study indicate that compounds from *Benincasa hispida*, particularly those targeting the identified key pathways and targets, could significantly impact the treatment or management of obesity and

IBD. The involvement of pathways related to the PI3K-Akt signaling pathway, insulin signaling pathway, mTOR signaling pathway, AMPK signaling pathway, adipocytokine signaling pathway and other pertinent pathways suggests a multifaceted approach to address the underlying molecular mechanisms of these diseases[39,41,42]. Molecular docking and dynamics studies provide an in-depth understanding of the interaction between Ajmalin and the MTOR protein. Docking studies revealed Ajmalin as the ligand with the highest binding affinity to MTOR, with a binding energy of -7.8 kcal/mol. The key residues involved in the interaction included HIS1670, ASN1703, MET1704, HIS1716, SER1707, and LEU1685, which allow strong binding via hydrogen bonds and hydrophobic contacts (Fig. 5). In contrast, dihydrocapsaicin and orlistat showed weaker affinities of -5.8 kcal/mol and − 5.2 kcal/mol, respectively, by engaging distinct residues. These results underscore the superior potential of Ajmalin to modulate MTOR activity effectively by forming stable and specific interactions at the binding site. Exploiting the docking results, molecular dynamics simulations were further conducted to investigate the stability and behavior of the Ajmalin-MTOR complex over a period of time. The RMSD analysis of the complex indicated stabilization after ~ 75 ns with minimal fluctuations thereafter, indicating a stable ligand configuration within the binding pocket. This finding is also consistent with the docking results since the identified interactions maintain stability during the simulation. The RMSF analysis also revealed that the binding of Ajmalin inhibited dynamic fluctuations in crucial areas of MTOR, implying a tight and stable interaction. These results confirm that the docking-predicted interactions are maintained under dynamic conditions, which further strengthens the hypothesis of the strong affinity of Ajmalin for MTOR.

Additionally, the radius of gyration (Rg) analysis highlighted the compactness of the protein–ligand complex, with consistent Rg values (~ 1.45 nm) throughout the 200 ns simulation. This compactness correlates with the high binding affinity of Ajmalin observed during docking, as stable binding likely prevents significant structural perturbations in MTOR. The SASA remained steady at ~ 500 nm^2 throughout the simulation. This finding indicates that the Ajmalin-MTOR complex is well adapted to the solvent environment without any notable destabilization. Finally, the binding energy values obtained from the MD simulations via the MMPBSA method confirmed the docking predictions. The average binding energy value of -16.596 ± 11.889 kJ/mol, which is supported by a strong van der Waals contribution of -85.72 ± 8.983 kJ/mol, indicates that Ajmalin interacts with MTOR through energetically favorable interactions. These results, when combined with docking data, present a holistic view of the interaction mechanism. In summary, the docking studies revealed that Ajmalin is the most potent ligand for MTOR, with the highest binding affinity and specific interactions involving crucial residues. This result is further supported by MD simulations, which show the stable and compact nature of the Ajmalin-MTOR complex under dynamic conditions. Taken together, these complementary analyses strongly suggest that Ajmalin could be a promising modulator of MTOR activity. Kang et al.. (2022) utilized LEPR subdomains with the PDB ID 3V6O in their in silico investigation to identify potential therapeutic drugs. Docking experiments of Ishophloroglucin A with the target subdomains revealed interactions with the residues Leu471, Tyr472, Leu505, and Leu506 in the active site of the CRH2 structure, as well as with the residue Cys6 of IGD[43]. This in silico study sought to determine whether *Benincasa hispida* Thunb extract could help reduce obesity-related inflammatory bowel disease (IBD). Chronic inflammatory conditions that affect the gastrointestinal tract, most notably Crohn's disease and ulcerative colitis, are called "inflammatory bowel disease"[44]. These conditions have many facets and are influenced by a variety of factors, including genetics, the environment, and immune system dysfunction. Although the specific cause of IBD is not yet fully understood, recent studies point to a potential link between obesity and the development or progression of IBD[45]. For the treatment of IBD, a variety of drugs are currently available, including steroidal and nonsteroidal anti-inflammatory drugs (NSAIDs) and immune-modulating biological agents that target particular pathways, such as interleukin-1 receptor and TNF- inhibitors. Unfortunately, several serious side effects are frequently associated with the use of common medications for gastrointestinal conditions, hemorrhage, and obesity. To determine the effect of *Benincasa hispida*, an in vivo study was performed with Wistar rats. Microplastics and monosodium glutamate (MSG) have each been studied separately in relation to a variety of health problems, such as obesity and inflammatory bowel disease (IBD)[10,46].

In the present study, the effects of microplastics and MSG on the well-being of Wistar rats were examined. A 28-day experimental study was conducted to examine the potential therapeutic benefits of *Benincasa hispida* extracts in reducing obesity-related inflammatory bowel disease (IBD). Compared with those in the control group, the body weights of the MSG-treated rats were significantly greater, whereas those of the MSG-treated rats displayed a more gradual decrease in weight. In the case of the microplastic-exposed group, treatment with the extracts led to a significant reduction in body weight and gradual recovery. One of the previous studies linked MSG consumption to weight gain and obesity because of its potential impact on appetite regulation and energy metabolism[47]. Conversely, the administration of *Benincasa hispida* extracts to the experimental groups yielded intriguing outcomes. The rats given these extracts exhibited a gradual reduction in body weight, suggesting a potential role in supporting weight management. These effects could be attributed to the bioactive compounds present in these plants, which have been reported to have anti-inflammatory and metabolic-regulating properties[48]. Notably, in the microplastic-exposed group, the use of extracts resulted in a significant reduction in body weight and gradual recovery, indicating the potential of these extracts to counteract the adverse effects of microplastic exposure.

Furthermore, to calculate the amount of lipids extracted from the feces, fecal matter testing was performed. IBD patients might have imbalances in particular lipid classes, such as too many proinflammatory lipids or not enough anti-inflammatory lipids[49]. Fecal lipid analysis can be used to identify these changes, as well as possible therapeutic targets and underlying mechanisms. Similarly, fecal lipid analysis in obesity can help in comprehending how lipid metabolism and the gut microbiota interact during the onset and progression of the disease. Fecal lipid analysis can pinpoint specific lipid-related indicators linked to obesity, enabling customized interventions or therapies[50]. Compared with the control and extract-treated groups, the MSG- and microplastic-treated groups presented higher levels of lipids.

Histopathological examination of the liver and intestine provided valuable insights into the inflammatory changes associated with different experimental conditions. In the liver histology of the normal and treatment groups, the absence of sinusoidal congestion, venous congestion, inflammation, fatty changes, or ballooning degeneration indicated a healthy physiological state. However, the MSG-induced group exhibited severe venous and sinusoidal congestion, ballooning degeneration, moderate fatty changes, and slight inflammation in the liver. These observations are in line with those of previous studies that highlighted the potential of MSG to induce liver alterations, inflammation, and steatosis[51]. Furthermore, the microplastic-induced group displayed distinct liver histology, featuring moderate sinusoidal congestion and fatty changes, mild inflammation, severe venous congestion and ballooning degeneration. These results underscore the intricate relationship between microplastic exposure and liver pathophysiology, corroborating studies that have suggested a potential link between microplastics and hepatic alterations[9]. However, there was no inflammation or fatty changes in the treatment groups, and only mild sinusoidal and venous congestion was observed. Similarly, histopathological examination of the intestine revealed significant differences between the groups. The MSG-induced group displayed severe inflammation, villous destruction, edema, epithelial exfoliation, and ulceration, which is consistent with the known proinflammatory effects of MSG on intestinal health. On the other hand, the microplastic-induced group exhibited a range of changes, including mild edema, moderate villous destruction, epithelial exfoliation, severe congestion, inflammation, and ulceration, further emphasizing the detrimental impact of microplastics on gut integrity. The treatment groups, however, exhibited milder changes, predominantly mild to moderate congestion without substantial villous damage or epithelial exfoliation. These findings highlight the potential ameliorative effects of *Benincasa hispida* extracts on inflammatory changes in the intestine. Future studies could explore the underlying mechanisms through which this extract exerts its protective effects on liver and intestinal histology. In conclusion, the histopathological examination underscores the significance of the observed inflammatory changes induced by MSG and microplastics in both the liver and intestine. The potential protective effects of plant extracts provide promising avenues for addressing these inflammatory alterations and warrant further mechanistic investigations.

Conclusions

The LCMS, in silico and in vivo findings of this comprehensive study reveal that *Benincasa hispida* (Thunb) Cogn is a potential candidate for the treatment of obesity-associated IBD on the basis of its ability to attenuate weight loss, reduce inflammation, and attenuate congestion in the liver and intestine of rats. Additionally, the results of network pharmacology and molecular docking have shown that there are important phytoconstituents present in *Benincasa hispida* that can be used to address the intricate challenges of obesity and inflammatory bowel disease. Thus, *Benincasa hispida* (Thunb) Cogn has wide future prospects in the development of novel therapeutic approaches for the treatment of obesity associated with IBD.

Data availability

All data generated or analysed during this study are included in this published article.

Received: 29 October 2024; Accepted: 18 April 2025
Published online: 25 April 2025

References

1. Jurjus, A. R., Khoury, N. N. & Reimund, J. M. Animal models of inflammatory bowel disease. *J. Pharmacol. Toxicol. Methods*. **50**, 81–92 (2004).
2. Chooi, Y. C., Ding, C. & Magkos, F. The epidemiology of obesity. *Metabolism* **92**, 6–10 (2019).
3. Harper, J. W. & Zisman, T. L. Interaction of obesity and inflammatory bowel disease. *World J. Gastroenterol.* **22**, 7868 (2016).
4. Greenfield, J. R. et al. Obesity is an important determinant of baseline serum C-Reactive protein concentration in monozygotic twins, independent of genetic influences. *Circulation* **109**, 3022–3028 (2004).
5. Catana, C. et al. Comparison of two models of inflammatory bowel disease in rats. *Adv. Clin. Exp. Med.* **27**, 599–607 (2018).
6. Parasuraman, S., Zhen, K., Banik, U. & Christapher, P. Ameliorative effect of Curcumin on olanzapine-induced obesity in Sprague-Dawley rats. *Pharmacognosy Res.* **9**, 247 (2017).
7. Lacruz, A., Baptista, T., de Mendoza, S., Mendoza-Guillén, J. M. & Hernández, L. Antipsychotic drug-induced obesity in rats: correlation between leptin, insulin and body weight during sulpiride treatment. *Mol. Psychiatry*. **5**, 70–76 (2000).
8. Angelova, P. & A REVIEW ON THE MODELS OF OBESITY, N. B. AND METABOLIC SYNDROME IN RATS. *Trakia J. Sci.* **1**, 5–12 (2013).
9. Liu, S., Li, H., Wang, J., Wu, B. & Guo, X. Polystyrene microplastics aggravate inflammatory damage in mice with intestinal immune imbalance. *Sci. Total Environ.* **833**, 155198 (2022).
10. Hernández Bautista, R. J., Mahmoud, A. M. & Königsberg, M. López Díaz Guerrero, N. E. Obesity: pathophysiology, monosodium glutamate-induced model and anti-obesity medicinal plants. *Biomed. Pharmacother.* **111**, 503–516 (2019).
11. Nahok, K. et al. Monosodium glutamate induces changes in hepatic and renal metabolic profiles and gut Microbiome of Wistar rats. *Nutrients* **13**, 1865 (2021).
12. Santana, P. T., Rosas, S. L. B., Ribeiro, B. E., Marinho, Y. & de Souza, H. S. P. Dysbiosis in inflammatory bowel disease: pathogenic role and potential therapeutic targets. *Int. J. Mol. Sci.* **23**, 3464 (2022).
13. Zaini, N. A. M., Anwar, F., Hamid, A. A. & Saari, N. Kundur [Benincasa hispida (Thunb.) Cogn.]: A potential source for valuable nutrients and functional foods. *Food Res. Int.* **44**, 2368–2376 (2011).
14. Al-Snaf, A. E. The Pharmacological importance of Benincasa hispida. A review. *Int. J. Pharma Sci. Res.* **4**, 165-170 (2013).
15. Kumar, A. Possible anorectic effect of methanol extract of possible anorectic effect of methanol extract of possible anorectic effect of methanol extract of Benincasa Benincasa hispida hispida hispida (Thunb). Cogn, fruit. *Indian J. Pharmacol.* **36**, 348–350 (2004).
16. NOR, M. K. & A. B. M. EXTRACTION OF BIOACTIVE COMPOUND *FROM PULP AND ROOTS OF Benincasa hispida A.k.a* (KUNDUR. (UNIVERSITI MALAYSIA PAHANG, 2013).
17. Muddapur, U. M. et al. Exploring bioactive phytochemicals in Gymnema sylvestre: biomedical uses and computational investigations. *Separations* **11**, 50 (2024).

18. David, A., Islam, S., Tankhilevich, E. & Sternberg, M. J. E. The alphafold database of protein structures: A biologist's guide. *J. Mol. Biol.* **434**, 167336 (2022).
19. Mohanraj, K. et al. IMPPAT: A curated database of Indian medicinal plants, phytochemistry and therapeutics. *Sci. Rep.* **8**, 4329 (2018).
20. Sun, W. et al. Material basis and molecular mechanisms of Dachengqi Decoction in the treatment of acute pancreatitis based on network Pharmacology. *Biomed. Pharmacother.* **121**, 109656 (2020).
21. Gfeller, D. et al. SwissTargetPrediction: a web server for target prediction of bioactive small molecules. *Nucleic Acids Res.* **42**, W32–W38 (2014).
22. Kuhn, M., von Mering, C., Campillos, M., Jensen, L. J. & Bork, P. STITCH: interaction networks of chemicals and proteins. *Nucleic Acids Res.* **36**, D684–D688 (2007).
23. Bai, L. L., Chen, H., Zhou, P. & Yu, J. Identification of tumor necrosis Factor-Alpha (TNF-α) inhibitor in rheumatoid arthritis using network Pharmacology and molecular Docking. *Front. Pharmacol.* **12**, 690118 (2021).
24. Zhang, F., Wu, J., Shen, Q., Chen, Z. & Qiao, Z. Investigating the mechanism of Tongqiao Huoxue decotion in the treatment of allergic rhinitis based on network Pharmacology and molecular docking: A review. *Med. (Baltim).* **102**, e33190 (2023).
25. Deshpande, S. H. et al. Silico study on the interactions, molecular docking, dynamics and simulation of potential compounds from Withania somnifera (L.) Dunal root against Cancer by targeting KAT6A. *Molecules* **28**, 1117 (2023).
26. Yaraguppi, D. A. et al. Identification of potent natural compounds in targeting leishmania major CYP51 and GP63 proteins using a high-throughput computationally enhanced screening. *Futur J. Pharm. Sci.* **6**, 18 (2020).
27. Mane, R. R., Yaraguppi, D. A., Bagewadi, Z. K. & Kamanna, K. Organocatalysed synthesis of N-(4-oxo-2-phenyl-1,2-dihydroquinazolin-3(4H)-yl)isonicotinamide: computational, electrochemical, drug-likeness and antimicrobial studies. *3 Biotech.* **15**, 30 (2025).
28. Percie du Sert. The ARRIVE guidelines 2.0: updated guidelines for reporting animal research. *PLOS Biol.* **18**, e3000410 (2020).
29. Haidari, F., Zakerkish, M., Borazjani, F. & Ahmadi Angali, K. Amoochi Foroushani, G. The effects of Anethum graveolens (dill) powder supplementation on clinical and metabolic status in patients with type 2 diabetes. *Trials* **21**, 483 (2020).
30. Kraus, D., Yang, Q. & Kahn, B. Lipid Extraction from Mouse Feces. *BIO-PROTOCOL* 5, (2015).
31. Abd El Maguid. Histological study of liver and intestine of rats treated with Colchicine. *Egypt. J. Hosp. Med.* **23**, 277–286 (2006).
32. Nanda, A., Mohapatra, D. B. B., Mahapatra, A. P. K., Mahapatra, A. P. K. & Mahapatra, A. P. K. Multiple comparison test by Tukey's honestly significant difference (HSD): do the confident level control type I error. *Int. J. Stat. Appl. Math.* **6**, 59–65 (2021).
33. Kanehisa, M., Furumichi, M., Sato, Y., Matsuura, Y. & Ishiguro-Watanabe, M. KEGG: biological systems database as a model of the real world. *Nucleic Acids Res.* **53**, D672–D677 (2025).
34. Kanehisa, M., Furumichi, M., Sato, Y., Kawashima, M. & Ishiguro-Watanabe M. KEGG for taxonomy-based analysis of pathways and genomes. *Nucleic Acids Res.* **51**, D587–D592 (2023).
35. Kanehisa, M. Toward Understanding the origin and evolution of cellular organisms. *Protein Sci.* **28**, 1947–1951 (2019).
36. Kanehisa, M. K. E. G. G. Kyoto encyclopedia of genes and genomes. *Nucleic Acids Res.* **28**, 27–30 (2000).
37. Banerjee, P., Eckert, A. O., Schrey, A. K. & Preissner, R. ProTox-II: a webserver for the prediction of toxicity of chemicals. *Nucleic Acids Res.* **46**, W257–W263 (2018).
38. Fruman, D. A. et al. The PI3K pathway in human disease. *Cell* **170**, 605–635 (2017).
39. Tanti, J. F., Ceppo, F., Jager, J. & Berthou, F. Implication of inflammatory signaling pathways in obesity-induced insulin resistance. *Front. Endocrinol. (Lausanne)* **3**, 181 (2013).
40. Chu, H. et al. MC-LR aggravates liver lipid metabolism disorders in obese mice fed a High-Fat diet via PI3K/AKT/mTOR/SREBP1 signaling pathway. *Toxins (Basel)* **14**, 833 (2022).
41. Onizawa, M. et al. Signaling pathway via TNF-α/NF-κB in intestinal epithelial cells May be directly involved in colitis-associated carcinogenesis. *Am. J. Physiol. Liver Physiol.* **296**, G850–G859 (2009).
42. Mukherjee, P. K., Banerjee, S. & Kar, A. Molecular combination networks in medicinal plants: Understanding synergy by network Pharmacology in Indian traditional medicine. *Phytochem Rev.* **20**, 693–703 (2021).
43. Kang, N. et al. Anti-obesity effects of Ishophloroglucin A from the brown seaweed ishige Okamurae (Yendo) via regulation of leptin signal in Ob/ob mice. *Algal Res.* **61**, 102533 (2022).
44. Satsangi, J., Jewell, D. P., Rosenberg, W. M. & Bell J. I. Genetics of inflammatory bowel disease. *Gut* **35**, 696–700 (1994).
45. Emerenziani, S. et al. Role of overweight and obesity in Gastrointestinal disease. *Nutrients* **12**, 111 (2019).
46. Souza-Silva, T. G. et al. Impact of microplastics on the intestinal microbiota: A systematic review of preclinical evidence. *Life Sci.* **294**, 120366 (2022).
47. He, K. et al. Association of monosodium glutamate intake with overweight in Chinese adults: the INTERMAP study. *Obesity* **16**, 1875–1880 (2008).
48. Gill, N. S., Dhiman, K., Bajwa, J., Sharma, P. & Sood, S. Evaluation of free radical scavenging, Anti-inflammatory and analgesic potential of Benincasa hispida seed extract. *Int. J. Pharmacol.* **6**, 652–657 (2010).
49. Das, U. N. Inflammatory bowel disease as a disorder of an imbalance between pro- and anti-inflammatory molecules and deficiency of resolution bioactive lipids. *Lipids Health Dis.* **15**, 11 (2016).
50. Joossens, M. et al. Dysbiosis of the faecal microbiota in patients with Crohn's disease and their unaffected relatives. *Gut* **60**, 631–637 (2011).
51. Hernández-Bautista, R. et al. Biochemical alterations during the Obese-Aging process in female and male monosodium glutamate (MSG)-Treated mice. *Int. J. Mol. Sci.* **15**, 11473–11494 (2014).

Acknowledgements

The authors extend their appreciation to University Higher Education Fund for funding this research work under Research Support Program for Central labs at King Khalid University through the project number CL/CO/A/3.

Author contributions

SBP and DAY have been involved in the concept design. SBP and DAY have executed all the research work. SBP, MBK, DAY, DP, SGH, GBT, and MAJ have analyzed and interpreted all the data. MBK, DAY, and SGH have written the manuscript. SBP and DAY have critically reviewed the manuscript. SBP and DAY have supervised the entire work. MAJ and TYK were involved in funding. All the authors have read and approved the contents of the manuscript.

Declarations

Competing interests

The authors declare that they do not have any conflicts of interest related to the current study or the

manuscript.

Ethical approval

The Institutional Animal Ethics Committee (IAEC) reviewed and approved the proposed animal study (Approval No. Mph/NC0221004/KLECoPH/22), as per the guidelines of the Committee for Control and Supervision of Experiments on Animals (CCSEA) in India.

Additional information

Correspondence and requests for materials should be addressed to D.A.Y.

Reprints and permissions information is available at www.nature.com/reprints.

Publisher's note Springer Nature remains neutral with regard to jurisdictional claims in published maps and institutional affiliations.